Therapeutic advantages of combined gene/cell therapy strategies in a murine model of GM2 gangliosidosis

Davide Sala,[1,5] Francesca Ornaghi,[1,5] Francesco Morena,[2] Chiara Argentati,[2] Manuela Valsecchi,[3] Valeria Alberizzi,[4] Roberta Di Guardo,[4] Alessandra Bolino,[4] Massimo Aureli,[3] Sabata Martino,[2] and Angela Gritti[1]

[1]San Raffaele Telethon Institute for Gene Therapy (SR-Tiget), IRCCS San Raffaele Scientific Institute, Via Olgettina 60, 20132 Milan, Italy; [2]Department of Chemistry, Biology, and Biotechnology, University of Perugia, Via del Giochetto, 06123 Perugia, Italy; [3]Department of Medical Biotechnology and Translational Medicine, University of Milano, Via Fratelli Cervi 93, 20090 Segrate, MI, Italy; [4]Division of Neuroscience, San Raffaele Scientific Institute, INSPE, Via Olgettina 58, 20132 Milan, Italy

Genetic deficiency of β-N-acetylhexosaminidase (Hex) functionality leads to accumulation of GM2 ganglioside in Tay-Sachs disease and Sandhoff disease (SD), which presently lack approved therapies. Current experimental gene therapy (GT) approaches with adeno-associated viral vectors (AAVs) still pose safety and efficacy issues, supporting the search for alternative therapeutic strategies. Here we leveraged the lentiviral vector (LV)-mediated intracerebral (IC) GT platform to deliver Hex genes to the CNS and combined this strategy with bone marrow transplantation (BMT) to provide a timely, pervasive, and long-lasting source of the Hex enzyme in the CNS and periphery of SD mice. Combined therapy outperformed individual treatments in terms of lifespan extension and normalization of the neuroinflammatory/neurodegenerative phenotypes of SD mice. These benefits correlated with a time-dependent increase in Hex activity and a remarkable reduction in GM2 storage in brain tissues that single treatments failed to achieve. Our results highlight the synergic mode of action of LV-mediated IC GT and BMT, clarify the contribution of treatments to the therapeutic outcome, and inform on the realistic threshold of corrective enzymatic activity. These results have important implications for interpretation of ongoing experimental therapies and for design of more effective treatment strategies for GM2 gangliosidosis.

INTRODUCTION

Genetic defects in the β-N-acetylhexosaminidase (Hex) enzyme cause GM2 gangliosidoses, a group of rare neurodegenerative lysosomal storage diseases (LSDs). This enzymatic deficiency leads to accumulation of GM2 and other glycosphingolipids in the central nervous system (CNS) and other organs.[1] Hex enzymes are found in three isoenzymes, resulting from variations in the association of different α and β subunits (HexA, αβ; HexB, ββ; HexS, αα) encoded by the HEXA (mutated in Tay-Sachs disease [TSD]) and HEXB genes (mutated in Sandhoff disease [SD]). The infantile forms of GM2 gangliosidosis are the most clinically common types and are extremely severe, but attenuated juvenile and late-onset forms also occur.[2–4]

There are currently no treatments for GM2 gangliosidosis. Enzyme replacement therapy,[5,6] substrate reduction therapy,[7,8] and pharmacological chaperones[9,10] provide partial benefits in cases of the juvenile/late-onset forms but are ineffective in infantile individuals.[11–16] Bone marrow transplantation (BMT) ameliorates neuroinflammation and prolongs the lifespan of SD mice ($Hexb^{-/-}$), which develop a progressive and severe neurological phenotype resulting in death at around 4 months of age.[17] However, BMT fails to supply therapeutic levels of Hex to CNS tissues[18,19] and provides minimal benefit for individuals with TSD or SD.[20,21]

Gene therapy (GT) holds promise as a means to address TSD and SD pathology. *In vivo* intracerebral (IC) GT, delivering functional Hex enzymes by means of adeno-associated viral vectors (AAVs), has benefited SD mice and cats[22–26] and is currently under clinical testing for infantile individuals[27] (ClinicalTrials.gov: NCT04798235 and NCT04669535). Despite this, pre-clinical studies and clinical observations have highlighted several major issues associated with this strategy; i.e., the necessity to co-deliver the α and β subunits at the appropriate ratio to achieve a fully functional enzyme, toxicity associated with Hex overexpression in brain cells upon IC GT,[28] immunogenicity of AAVs that require some immunosuppressive treatment to support durable transgene expression,[29,30] and potential off-target toxicity because of AAV leakiness,[31] which requires long-term efficacy and safety evaluations. Lentiviral vectors (LVs) transduce neuronal and glial cells with high efficiency and display little dispersion and low immunogenicity upon IC delivery,[32,33] representing a complementary/alternative GT platform to target the CNS. The results of the first clinical trial using an LV-based GT vector to treat individuals with Parkinson's disease showed a favorable safety profile

Correspondence: Angela Gritti, San Raffaele Telethon Institute for Gene Therapy (SR-Tiget), IRCCS San Raffaele Scientific Institute, Via Olgettina 60, 20132 Milan, Italy.
E-mail: gritti.angela@hsr.it

and indication of efficacy.[34,35] We have previously shown the safety and efficacy of an LV-based IC GT platform to provide stable levels of therapeutic lysosomal enzymes in murine and non-human primate models of leukodystrophies.[32,33,36] In addition, we have generated mono- and bicistronic LVs driving the expression of Hex genes in neural and hematopoietic cells,[37] supporting the rationale of testing these LVs in GT platforms to treat GM2 gangliosidosis.

Low levels of GM2 storage may affect developing neurons and glial cells, greatly restricting the time window available for effective therapeutic interventions. Indeed, neurodevelopmental defects have been described in GM2 gangliosidosis[38–40] as well as other infantile neurodegenerative LSDs; e.g., mucopolysaccharidosis type 1 (MPSI), Nieman-Pick disease[41,42] and globoid cell leukodystrophy (GLD).[43,44] In addition to the timing of the intervention, the threshold concentration of enzyme needed for a therapeutic effect is a central issue for consideration. It is widely assumed that 10%–15% of normal enzymatic activity is sufficient to hydrolyze excess substrates and prevent disease manifestations in various LSDs, including GM2 gangliosidosis.[2,45,46] However, whether a treatment ensures that these enzymatic levels are met on a per-cell basis in animal models and individuals needs to be clarified. In addition, the early neuroinflammation and myelin dysfunction described in GM2 gangliosidosis animal models and affected individuals[19,22,47,48] suggest that a therapy able to limit and prevent tissue damage and promote repair, in addition to restoring an endogenous source of functional enzyme, is required. Finally, despite TSD and SD primarily affecting the CNS, approaches that provide additional enzymatic correction and neuroprotection to the peripheral nervous system (PNS) and peripheral organs would likely enhance the therapeutic benefits. Variable synergy in terms of clearance of storage, survival, and functional rescue has been described when combining oral glycosphingolipid biosynthesis inhibitors with neural stem cell transplantation (NSCT)[49,50] or BMT.[51] We have shown previously that LV-mediated neonatal NSCT or IC GT synergizes with BMT, providing remarkable health benefits to a severe murine model of GLD.[52] The results of our study indicated that the early availability of functional enzyme promoted by NSCT and IC GT is instrumental for enhancing the long-term advantages of BMT. These findings provide a strong rationale to evaluate the therapeutic benefits of combined strategies based on IC GT and BMT in GM2 gangliosidosis diseases, which share with GLDs the problems of early onset, rapid progression, severe CNS damage, and limitations of the benefits achieved after experimental therapies are applied individually.

To address the safety and efficacy issues of GT approaches currently being developed (such as in vivo AAV GT), we aimed to evaluate the potential of using the LV-mediated GT platform to deliver Hex genes to the CNS and demonstrate the potential of combining this strategy with BMT to prevent/delay disease onset and progression, prolong the lifespan, and correct pathological hallmarks of SD mice. We demonstrate that sequential administration of LV-mediated IC GT and BMT in pre-symptomatic SD mice provides a timely and long-lasting source of Hex and confers neuroprotection/immunomodulation in the CNS, PNS, and periphery. Combined therapy comes with remarkable advantages compared with individual treatments in terms of extending the lifespan of SD mice and global rescue of the disease phenotype. These benefits rely on the complementary modality of the treatments' mechanisms of action and correlate with increased enzymatic activity and a significant reduction in GM2 storage in CNS tissues.

This work demonstrates the suitability of using an LV-mediated GT platform to deliver Hex genes to the CNS and the overall therapeutic potential of the proposed combined strategy. The findings clarify the relative contribution of treatments to the therapeutic outcome and inform on the realistic threshold of enzymatic activity that is required to achieve a significant therapeutic benefit, with important implications for monitoring and interpretation of ongoing experimental therapies and for design of more effective treatment strategies for GM2 gangliosidosis.

RESULTS

Experimental plan

In this study, we took advantage of optimized experimental protocols for LV-mediated IC GT and BMT,[32,33,52,53] and the experimental plan is summarized in Figure 1. We used LVs to drive expression of the murine α and β Hex subunits under control of the human phosphoglycerate kinase (PGK) promoter (LV.hexB and LV.hexA).[37] Pilot experiments showed local rescue of enzyme activity and isoenzyme composition in the injected hemisphere but little enzymatic activity in the contralateral hemisphere upon unilateral LV injection (Figures S1A–S1C). Thus, we performed bilateral co-injections of purified LVs into the external capsule (EC) of post-natal day 2 SD mice ($Hexb^{-/-}$) (LV.hexB + LV.hexA, 2×10^6 transducing units (TU)/μL of each vector, 4 μL in total). In the combined treatment group, LV-injected mice were transplanted at 60 days of age with total bone marrow (BM) from transgenic green fluorescent protein (tgGFP)-expressing mice. Untreated (UT) mice, IC GT- and BMT-treated SD mice, UT wild-type (WT; $Hexb^{+/+}$), and heterozygous (Het; $Hexb^{+/-}$) age-matched littermates were used as controls. Mice were analyzed at different time points during disease progression and after treatment to assess (1) engraftment of transplanted cells and brain cell transduction upon IC GT, (2) Hex activity in the CNS, PNS, and peripheral organs, and (3) progression of disease-associated pathological features (lysosomal expansion, glycolipid storage, neuroinflammation, neurodegeneration, and myelin damage) and their treatment-associated rescue by means of a thorough molecular, biochemical, and morphological evaluation.

Synergy of treatments for increasing the lifespan of SD mice

The Kaplan-Meier survival curves for all treatment groups are shown in Figure 2A. UT SD mice followed a rapidly progressive neurodegenerative course, starting from around 90 days of age, and showed a median survival of 120 days (100–135 days, n = 93 mice). Single treatments resulted in a modest but significant increase in median survival, which were 132 days (118–143 days, n = 6) for IC GT and 136 days (122–180 days, n = 13) for BMT. Combination-treated SD mice lived
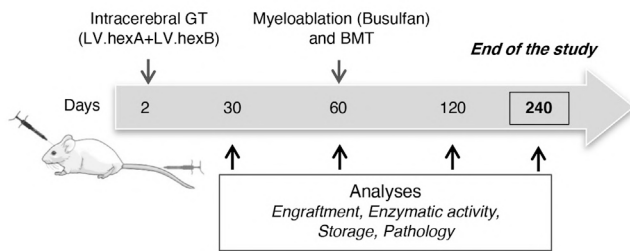
Figure 1. Experimental plan

LVs (LV.hexA+ LV.hexB) were co-injected bilaterally into the EC of neonatal mice at 2 days. Transplantation of total BM isolated from tgGFP WT donors was performed at 60 days of age after busulfan treatment (myeloablation). Untreated (UT) and/or treated SD mice (Hexb$^{-/-}$) were analyzed during disease progression (30 days, 60 days, asymptomatic; 120 days, terminal stage of disease) and after treatment (120 days; 240 days, end of the study). Intracerebral (IC) gene therapy (GT), BM transplantation (BMT), and combined (IC GT + BMT) treatments were applied to SD mice, WT (Hexb$^{+/+}$) and heterozygous (Het; Hexb$^{+/-}$) littermates.

significantly longer than UT SD and SD mice treated with individual approaches, with a mean survival of 210 days (142–246 days, n = 13, with six animals sacrificed at 240 days, the endpoint of the study). Despite the significant delay in onset of symptoms, IC GT- and BMT-treated SD mice experienced the rapid and severe disease progression that characterized the UT SD controls, eventually exhibiting muscle wasting, rigidity, and a nearly complete inability to ambulate. In contrast, the combined therapy resulted in strikingly improved clinical appearance at a time when the SD mice treated with BMT or IC GT alone, as well as UT controls, were severely affected with disease manifestations. All combination-treated SD mice (including the three animals sacrificed at 240 days) displayed only mild tremors and ataxia, maintained walking and explorative ability (Videos S1, S2, and S3), were able to feed independently, and showed preservation of normal body weight (Figure 2B).

Stable transduction of CNS cells and hematopoietic cell engraftment in combination-treated SD mice

Mice were examined to evaluate the efficacy of neural cell transduction upon IC GT (30 days after LV injection) and engraftment of BM-derived hematopoietic cells (HCs) in peripheral blood (PB) at 30 days and BM at 60 days after transplantation. In line with our previous studies,[52] we detected robust transduction of endogenous cells and widespread transgene diffusion along white matter tracts upon neonatal IC GT, which we assessed using LV.GFP delivery in a group of control animals (Figure S1D). Injection of LV.hexA + LV.hexB resulted in a decrease in GM2 storage and a reduction in cluster of differentiation 68 (CD68)$^+$ macrophages in areas of the brain close to the injection site (Figure 3A; 120 days), suggesting the functionality of the transgenic enzyme and the short range of action.

The pervasive engraftment of metabolically competent HCs into the CNS tissues of BMT-treated SD mice was expected to enhance the enzymatic supply to therapeutically benefit affected tissues. We applied busulfan as a conditioning regimen capable of ablating the resident hematopoietic niche as well as brain-resident myeloid precursors, favoring turnover from resident myeloid cells to the donor counterparts.[54] Cytofluorimetric analysis showed sustained and stable chimerism in BMT- and combination-treated SD mice (>90% and >60% of GFP$^+$ donor-derived HCs in the PB and BM, respec-

tively; Figures 3B and 3C), with complete reconstitution of white blood cell (WBC) and red blood cell (RBC) populations and normal WBC composition (Table S1). Transplanted mice and tgGFP donor mice showed comparable percentages of GFP$^+$ cells and BM cell type compositions (Figures 3C and 3D). These data suggest that Hex deficiency did not affect the engraftment of donor-derived HCs, which was stable over time and ensured functional hemopoiesis.

Immunofluorescence (IF) analysis of brain tissues of BMT- and combination-treated mice at 120 and 240 days showed robust, widespread, and time-dependent engraftment of donor-derived GFP$^+$ cells, which were distributed rostrocaudally in some areas of higher GFP$^+$ cell density (i.e., the olfactory bulbs, thalamus, pons, and medulla) (Figures 3E and 3F). A similar distribution of GFP$^+$ cells was found in BMT-treated (analyzed at 120 days of age) and combination-treated SD mice (analyzed at 120 and 240 days), suggesting that IC GT did not affect the modality of HC recruitment/engraftment in CNS tissues.

Enhanced reconstitution of Hex activity in CNS tissues of combination-treated SD mice

To evaluate the efficacy of in-vivo-transduced neural cells upon IC GT and donor-derived HC myeloid progeny upon BMT and IC GT + BMT to the supply of functional enzyme in the CNS and periphery, we measured Hex activity in the telencephalon (TEL), cerebellum (CB), spinal cord (SC), cerebrospinal fluid (CSF), BM, liver, spleen, and sciatic nerve (SN) of treated and UT SD mice using two artificial substrates: 3 mM 4-methyl-umbelliferyl-N-acetyl-β-d-glucosaminide (MUG), used to determine total Hex activity (HexA, HexB, and HexS), and 3 mM 4-methyl-umbelliferone-6-sulfo-2-acetamido-2-deoxy-β-d-glucopyranoside (MUGS), used to determine HexA activity. We analyzed cohorts of treated animals at 120 days (IC GT, BMT, and IC GT + BMT) and 240 days of age (IC GT + BMT) and included age-matched WT and Het groups as controls.

The CNS tissues of UT SD mice (120 days) displayed minimal residual enzymatic activity ($\leq$3% and $\leq$10% of physiological levels, assessed using MUG and MUGS, respectively) because of presence of the αα isoenzyme (Figures 4A and S2A–S2D). WT and Het mice showed a significant caudal-to-rostral increase in Hex activity in the CNS, with the highest values measured in the TEL compared with the CB and SC. Interestingly, we detected a significant
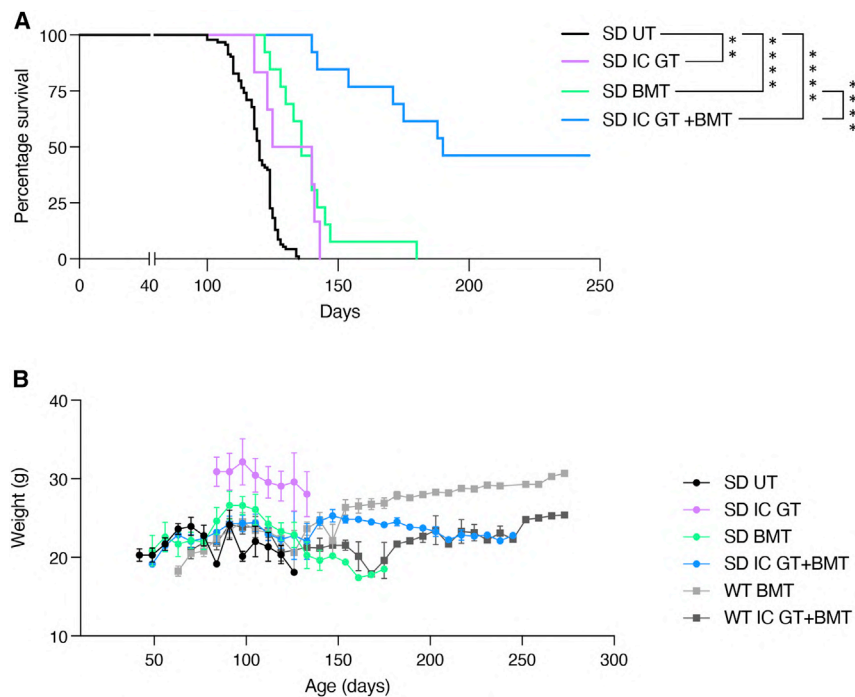
Figure 2. Synergy of treatments in increasing the lifespan and preserving the body weight of SD mice
(A) Kaplan-Meier survival curves showing the percentage survival of treated and UT SD mice. SD UT, n = 93; SD IC GT = 6; SD BMT, n = 13; SD IC GT + BMT, n = 12. Data were analyzed by log rank (Mantel-Cox) test: **p < 0.005, ****p < 0.0001. (B) Body weight of treated SD mice and UT littermates was monitored from 50 days of age. BMT-treated WT/Het mice were used as controls to evaluate the effect of busulfan conditioning on body weight. The higher body weight of IC GT-treated mice reflected the absence of the myeloablative regimen in this treatment group. Data represent the mean ± SEM; n = 5–19 mice/group.

age-associated increase in enzymatic activity in WT tissues (Figures 4B and S2A–S2D).

IC GT-treated SD mice analyzed at 120 days displayed a modest increase in enzymatic activity in the TEL ($\approx$7% of WT-MUG) but not in the CB or SC, suggesting poor diffusion of Hex away from the site of injection. In the CNS of BMT-treated mice, enzymatic reconstitution was low in the TEL ($\approx$5% of WT-MUG), increased in the CB ($\approx$20% of WT/MUG), and significantly higher in the SC ($\approx$65% of WT-MUG), likely reflecting caudal-to-rostral HC engraftment in CNS tissues (Figures 4A and S2A–S2C). The similar enzymatic activity recorded in the TEL of IC GT- and BMT-treated SD mice highlighted the modest but stable enzymatic supply provided by neonatal IC GT in this region, in which HC-derived myeloid reconstitution was delayed compared with that in caudal regions. Combination-treated SD mice showed higher Hex reconstitution compared with BMT-treated mice in the TEL and CB ($\approx$20% and $\approx$34% of WT-MUG, respectively) and a significant increase in the SC ($\approx$73% of WT-MUG) (Figures 4A and S2A–S2C). The presence of robust Hex activity in the CSF of combination-treated SD mice ($\approx$60% of WT-MUG) compared with IC GT- ($\approx$18% of WT-MUG) and BMT-treated mice ($\approx$34% of WT-MUG) (Figures 4A and S2A–S2C) confirmed the production and release of functional enzyme by LV-transduced neural cells and donor HC-derived brain myeloid cells. The synergy of the treatments became even more evident in combination-treated animals analyzed at 240 days of age, which showed stable Hex activity in the TEL and CB and physiological Hex levels in the SC (Figures 4A and S2A–S2C). Importantly, diethylaminoethyl (DEAE) chromatography performed on TEL tissues showed normal patterns of HexA and HexB isoenzymes in combination-treated SD mice (Figure S2E).

We next assessed enzymatic reconstitution in the BM niche and the time-dependent contribution of donor HC-derived myeloid progeny in providing functional Hex to the PNS and periphery. The normalization of enzymatic activity measured at 120 days and 240 days in the BM of BMT- and combination-treated SD mice confirmed the high and stable peripheral chimerism and complete reconstitution of the hematopoietic system 2 months after transplantation (Figures 4D and S2F). The high numbers of GFP⁺CD68⁺ macrophages detected in the liver (Figure 4E) and spleen (Figure 4F) of BMT-treated SD mice at 120 days was in line with the observed rescue of Hex activity to Het (liver) and WT enzymatic levels (spleen) (Figures 4G, 4H, S2G, and S2H). Interestingly, Hex activity in the SN of BMT-transplanted mice was rescued to Het (120 days), physiological, or supraphysiological levels (240 days) (Figures 4I and S2I), suggesting that the kinetics of the PNS macrophage replacement were comparatively slow. Enzymatic activity in the peripheral tissues of IC GT-treated SD mice was similar to that of UT SD controls, concurrent with previous studies showing the CNS-specific targeting of this approach.[33]

These results suggest that there was complete repopulation of spleen and liver macrophages by donor HC-derived myeloid progeny 2 months after BMT in SD mice. In contrast, at least 4 months were needed for significant repopulation of rostral brain regions, in which the requirement for enzymatic reconstitution was the highest. This timing is not very compatible with the rapid acceleration in disease progression experienced by these mice unless a complementary source of early enzymatic supply (in this case provided by IC GT) is available. Interestingly, a similar time frame was required for full repopulation of the PNS by HC-derived macrophages and maximum restoration of Hex activity.

Correction of lysosomal expansion and clearance of GM2 storage in the CNS of combined-treated mice

We next investigated whether the enzymatic rescue provided by the treatments would lead to amelioration/rescue of SD pathological hallmarks in CNS tissues. Increased expression of lysosome-associated
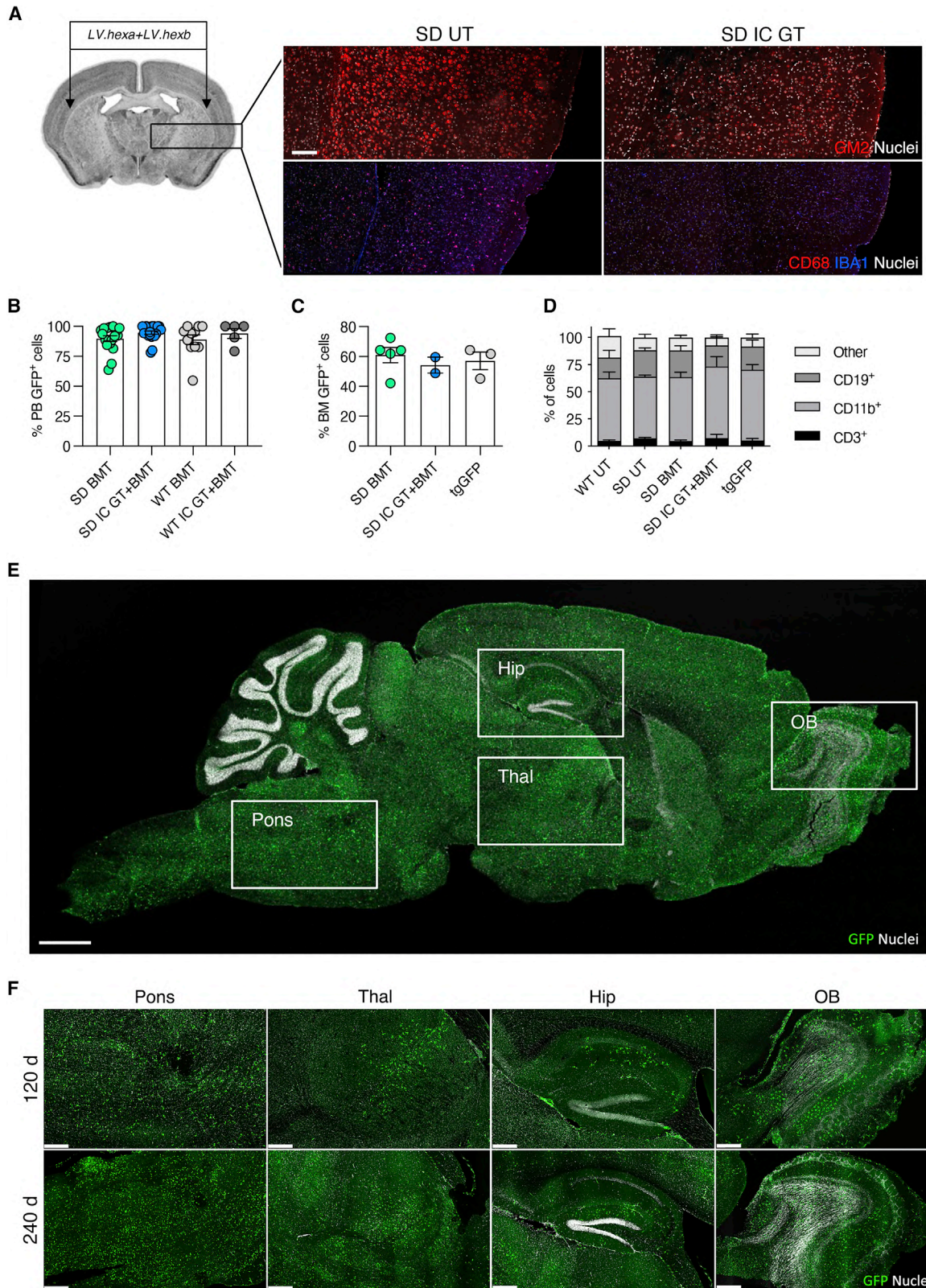
(legend on next page)

membrane protein 1 (LAMP1) is associated with lysosomal impairment in several LSDs.[55] We discovered significant age-dependent (120 days > 60 days > 30 days) and region-dependent (CB > SC > TEL) accumulation of LAMP1 protein in the CNS tissues of UT SD mice compared with the age-matched WT controls (4- to 10-fold higher than the WT levels; Figure S3), which was reduced or normalized in the brain of treated SD mice at 120 days and 240 days (Figure 5A). These results suggest that the age-dependent reduction in LAMP1 expression in CNS tissues is related to the increased supply of functional Hex provided over time by the treatment.

Hex deficiency significantly increases the concentrations of brain GM2 ganglioside and its asialo counterpart gangliotriaosylceramide (GA2), which are only present at trace concentrations under physiological conditions.[56] We detected increased GM2 and GA2 contents in the brain tissues of UT SD mice at 30 days and 60 days of age (i.e., the asymptomatic stage) compared with WT controls. In 120-day-old fully symptomatic mice, the GM2 ganglioside and GA2 contents were 28.7% ± 4.2% and 19.5% ± 4.5% of the total gangliosides and total neutral sphingolipids, respectively (Figures S4A and S4B). To evaluate the contribution of different therapies to preventing, delaying, and/or reducing the ganglioside store, we quantified GM2 and GA2 in brain tissue lysates of treated and UT SD mice compared with WT/Het controls. GM2 and GA2 storage was unchanged or slightly decreased in IC GT- and BMT-treated SD mice analyzed at 120 days of age. In contrast, combination-treated mice showed GM2 and GA2 levels similar to those measured in asymptomatic 30-day-old UT SD mice. This reduction was even more apparent in mice analyzed at 240 days of age (Figures 5B and 5C). Qualitative IF analysis of the brain tissue of treated mice and controls with an anti-GM2 antibody confirmed the efficacy of the combined treatment in clearing ganglioside storage (Figure 5D), specifically in brain regions such as the olfactory bulb, septum, and dentate gyrus, where GM2 accumulates first and most abundantly (Figure S4C).

The extent of residual GM2 and GA2 stores in the brain tissues of treated mice correlated with the level of Hex activity (Figure 5E). The modest enzymatic supply provided by IC GT or BMT (<10% of WT-MUG) resulted in minimal or no reduction in storage levels. In contrast, 20%–25% of the physiological Hex activity provided by combination treatment resulted in a remarkable reduction in GM2 and GA2 levels, with a tendency for improvement in 240-day-old-treated mice, in which GM2 and GA2 levels were reduced to 40%–50% of those detected in fully symptomatic UT SD animals (Figures 5B–5E).

These data conclusively showed that the enzymatic supply provided to CNS tissues by single-treatment IC GT or BMT fell below the threshold levels required for therapeutic benefit. The reduced, even if not normalized, storage levels in combination-treated mice suggests that supplying low levels of functional enzyme to the neonatal brain can foster long-term BMT-mediated therapeutic effects.

Amelioration of neuroinflammation by combined treatment

Astrogliosis and microgliosis contribute to onset and maintenance of the disease phenotype of several neurodegenerative diseases and may precede full manifestation of extensive neurodegeneration and demyelination in SD.[19,57] Time course qPCR and IF analyses performed on CNS tissues of asymptomatic (30 days and 60 days) and fully symptomatic (120 days) UT SD mice and age-matched WT controls showed disease- and age-dependent upregulation of inflammatory cytokines (*Mip-1a*/chemokine ligand 3 [*Ccl3*], *Rantes*/*Ccl5*) and macrophage (*Cd68*) and astrocyte (glial fibrillary acidic protein [*Gfap*]) markers (Figures S5A and S5B). BMT and combined treatments, but not IC GT, rescued *Ccl3*, *Ccl5*, and *Cd68* gene expression (Figure 6A), suggesting a major anti-inflammatory contribution of HC-derived myeloid cells in the SD brain. The pronounced astrogliosis observed in UT SD mice was partially reduced by combined treatment but not by BMT alone at 120 days and was stabilized at 240 days, as assessed at the mRNA (Figure 6A) and protein levels (Figure 6B).

Qualitative IF analysis performed on brain tissues of treated SD mice and controls showed persistent reduction of CD68^{+} immunoreactivity in SD mice that received IC GT + BMT (120 days and 240 days; Figure 6C). Importantly, resident and donor-derived (GFP^{+}) Iba1^{+} cells in combination-treated mice displayed a ramified, resting-like morphology as opposed to the ameboid shape associated with a phagocytic/activated state observed in tissues from UT SD mice.

These results highlighted the synergistic action of early IC GT and BMT against astrogliosis and microgliosis in the CNS of SD mice and in providing a long-term therapeutic advantage.

Figure 3. Transduction of neural cells upon IC GT and brain myeloid cell reconstitution upon BMT in SD mice

(A) Schematic of LV.hexA+ LV.hexBinjection and immunofluorescence (IF) confocal image showing clearance of GM2 storage and reduction in CD68^{+} cells in a region of SD brain tissue (box) close to the LV injection site. Top panel: GM2, red. Bottom panel: CD68, red; IBA1, blue. Nuclei are counterstained with Hoechst (white). Scale bar, 25 μm. (B and C) Percentages of donor-derived GFP^{+} cells in the peripheral blood (PB; B) and bone marrow (BM; C) of BMT- and IC GT + BMT-treated SD and WT mice evaluated 30 days (PB) and 60 days (BM) after BMT. The percentage of GFP^{+} cells in the BM of tgGFP mice (donors) is shown for comparison. (D) Cellular composition of the BM analyzed 60 days after transplantation into BMT- and IC GT + BMT-treated SD mice and age-matched UT controls (WT, SD, and tgGFP mice). CD19, marker for B cells; CD11b, marker for monocytes, neutrophils, and natural killer (NK) cells; CD3, marker of mature T cells. Data represent the mean ± SEM; n = 3–13 mice/group. (E) IF image showing the distribution of GFP^{+} cells in a whole brain sagittal section of an IC GT + BMT-treated SD mouse at 120 days. Boxes highlight brain regions in (F) at higher magnification. (F) IF pictures showing GFP^{+} cells engrafted into the olfactory bulb (OB), hippocampus (Hip), thalamus (Thal), and pons/medulla (Pons) of IC GT + BMT-treated SD mice at 120 days and 240 days. (E) and (F) Direct GFP fluorescence, green; nuclei counterstained with Hoechst, gray. Scale bars, 3,000 μm (E) and 500 μm (F).
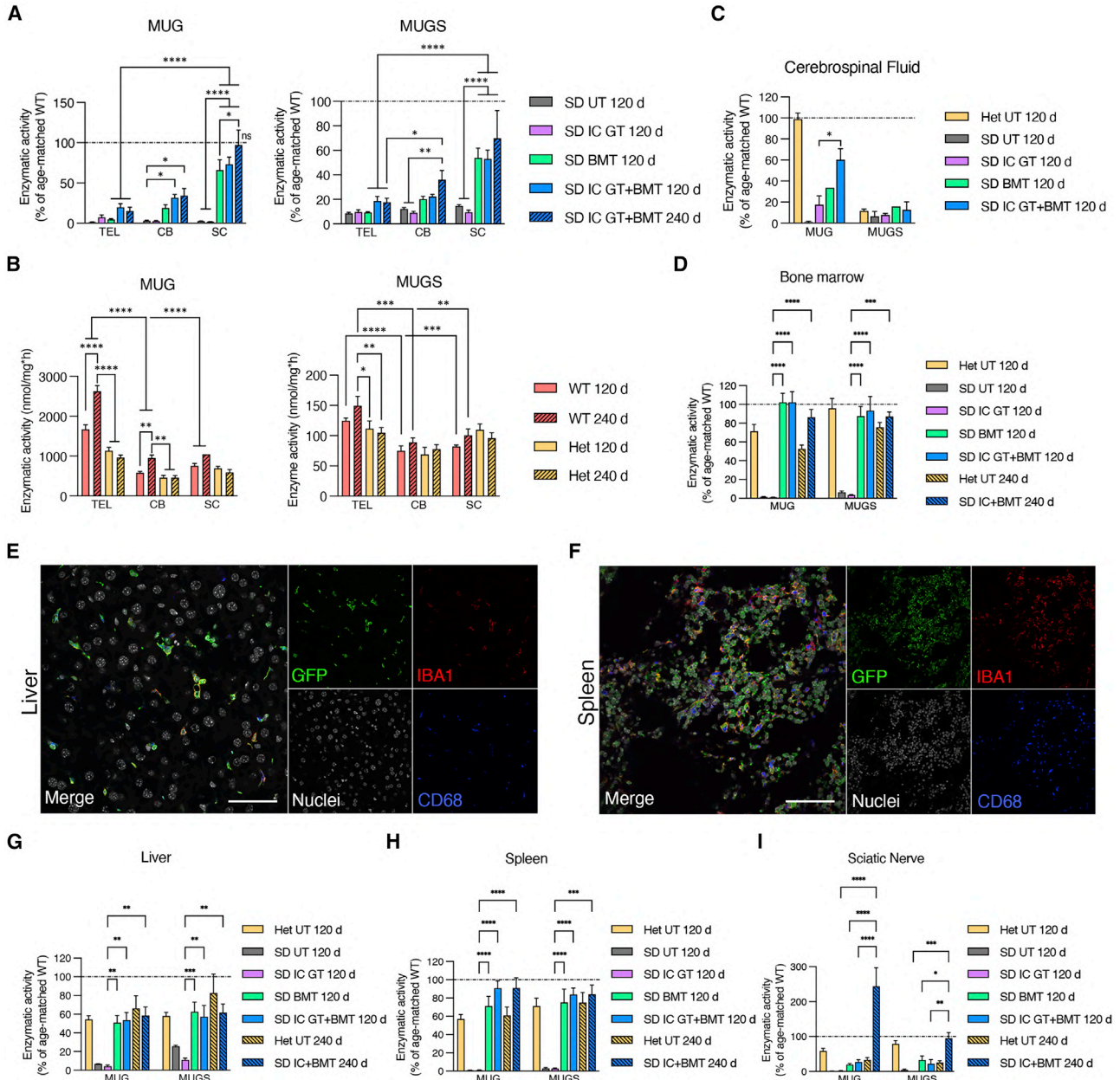
Figure 4. Hex enzymatic activity in CNS tissues, PNS, and periphery of treated SD mice and controls

(A) Enzymatic activity measured in the telencephalon (TEL), cerebellum (CB), and spinal cord (SC) tissues of IC GT-, BMT-, and IC GT + BMT-treated SD mice and age-matched UT SD mice at 120 days and 240 days. Enzymatic activity was measured as degradation of the artificial substrates MUG (left graph) and MUGS (right graph) and expressed as the percentage of age-matched UT WT control data. (B) Enzymatic activity (MUG, MUGS; expressed as nanomoles per milligram per hour) in the TEL, CB, and SC tissues of WT and Het mice at 120 days and 240 days. *$p < 0.01$, **$p < 0.005$, ***$p < 0.001$, ****$p < 0.0001$. (C and D) Enzymatic activity (MUG, MUGS; expressed as the percentage of age-matched UT WT controls) measured in the cerebrospinal fluid (CSF; (C) and BM (D) of treated SD mice (IC GT, BMT, and IC GT + BMT) and UT controls (Het and SD) at 120 days and 240 days. *$p < 0.05$ (C); ****$p < 0.0001$, ***$p < 0.001$ SD IC GT 120 days versus all other treatments (D). Combined treatment versus WT UT, not significant. (E and F) Confocal IF images showing donor-derived GFP$^+$ cells (green) expressing the microglial and macrophagic markers Iba1 (red) and CD68 (blue), respectively, in the liver (E) and spleen (F) of BMT-treated SD mice at 120 days. Scale bar, 50 μm. (G–I) Enzymatic activity measured in the liver (G), spleen (H), and sciatic nerve (I) of treated SD mice (IC GT, BMT, and IC GT + BMT) and UT controls (Het and SD) at 120 days and 240 days. Enzymatic activity was measured as degradation of MUG and MUGS and expressed as the percentage of age-matched UT WT controls. **$p < 0.01$, ****$p < 0.0001$ SD IC GT 120 days versus all other treatments (G and H). ****$p < 0.0001$, **$p < 0.01$ SD IC GT + BMT 240 days versus all other treatments (I). Combined treatment versus Het (liver) and WT (spleen), $p > 0.05$. Data in (A)–(D) and (G)–(I) are expressed as the mean ± SEM; n = 3–9 mice/group. Data were analyzed by two-way ANOVA followed by Tukey's multiple comparisons test.
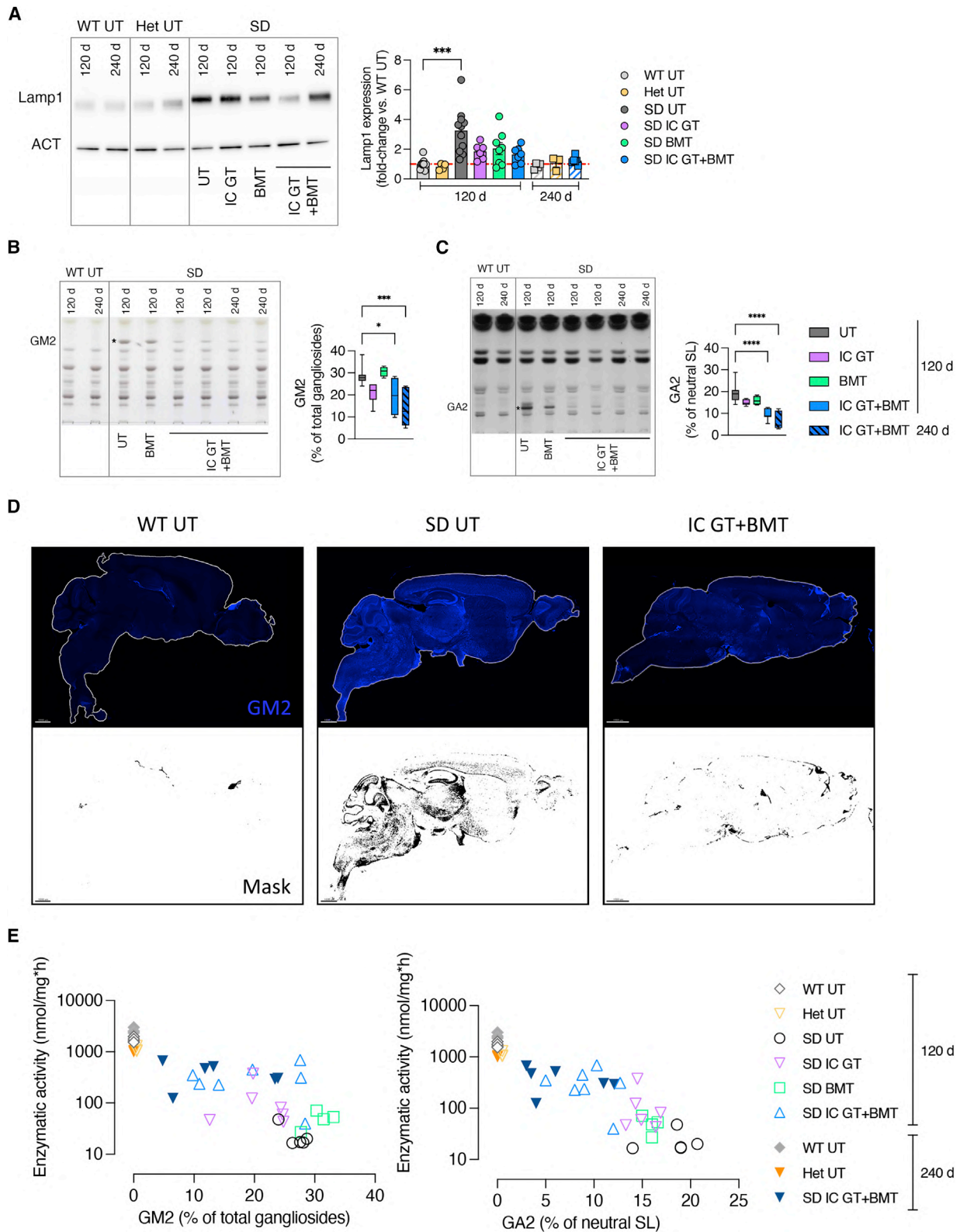
Transient rescue of Purkinje cell degeneration by combined treatment

The evident ataxic phenotype of fully symptomatic SD mice prompted us to investigate the potential cerebellar alterations. Qualitative IF analysis suggested that there was less prominent GM2 storage in the CB of SD mice compared with other brain regions (Figure S4C), with an evident GM2+ signal in the granular and molecular layers and apparent modest storage in Purkinje cells (PCs) (Figure 7A). The altered morphology of PC dendritic trees and the altered localization of calbindin protein in the PCs of 30-day-old and 60-day-old asymptomatic SD mice compared with age-matched WT mice suggested the occurrence of neuronal dysfunction and/or ongoing neurodegeneration (Figure 7B). Loss of PCs became evident in 120-day-old symptomatic SD mice, which exhibited an ≈25% reduction in PCs compared with the age-matched WT controls (Figure 7C). Importantly, the PC numbers, but not calbindin mis-localization or dendrite morphology, were transiently ameliorated in IC GT SD mice and normalized in BMT- and combination-treated animals (Figure 7D).

Partial rescue of myelin defects by combined treatment

In addition to the SD effects on neurons, defects in myelin structure and composition have been described in the CNS of SD animal models[56,58–60] and affected individuals.[61] To assess whether single and combined treatments are able to preserve and/or rescue myelin integrity in CNS tissues, we performed morphometric analysis of SC and optic nerves. We did not observe any defects in the myelin or axons of SD mutant SNs at 30 days or 120 days, confirming previous findings in the PNS.[62,63]

Semithin sections and ultrastructural analyses of cervical and lumbar SC regions of UT SD mice at 120 days revealed the presence of several fibers displaying demyelination and myelin degeneration. The total number of myelinated fibers and the axonal diameter distribution were similar in the mutants and controls (data not shown). However, the percentage of demyelinated/degenerated fibers within the total myelinated fibers was unchanged after BMT at 120 days and, importantly, after IC GT + BMT at 120 days and 240 days, suggesting that this strategy might inhibit disease progression and prevent further myelin deterioration (Figures 8A and 8B).

Electron microscopy analyses of the optic nerves of UT SD mice (120 days) revealed macrophage infiltration and signs of axonal degeneration (organelle swelling and accumulation of storage mate-

rials). Contrary to what was observed in the SC sections, this phenotype was aggravated in combination-treated SD mice at 240 days, a time when loss of myelinated fibers was observed (Figure 8C).

To support the morphological observations, we first analyzed the expression of myelin proteins in brain lysates from UT and treated SD mice at 120 days (IC GT, BMT, and IC GT + BMT) and 240 days (IC GT + BMT) by western blot, including age-matched WT and Het mice controls (Figure 8D). Quantification of the immunoblot bands showed a 40%–50% reduction in myelin basic protein (MBP) and myelin-associated glycoprotein (MAG) expression in UT SD mice compared with WT controls at 120 days of age. BMT and combined treatments (but not IC GT) rescued MBP expression, which was stable in combination-treated SD mice at 240 days. We observed a 50% reduction in MAG expression in 240-day-old compared with 120-day-old WT mice. Combination-treated SD mice analyzed at 240 days showed MAG levels similar to the age-matched WT controls. In line with a previous report,[60] we detected similar expression levels of the myelin genes *Mbp*, *Mag*, *Plp1* (proteolipid protein 1), and *Ugt8a* (UDP galactosyltransferase 8A) in brain tissues of UT SD mice and WT controls, and these levels were not significantly affected by the treatments (Figure 8E).

These data suggest that a disease-associated alteration in brain myelin protein composition can be rescued by combined therapy in SD mice, whereas it remains relatively refractory to correction by isolated therapies.

DISCUSSION

In this work, we showed the complementary modes of action and synergistic effects of LV-mediated IC GT and BMT in providing a significant therapeutic enzymatic supply and counteracting multiple pathological hallmarks in brain tissues of SD mice, which recapitulated the severity and rapid progression of early-onset forms of SD.

Combination-treated mice preserved their normal body weight and motor functions until 150 days of age, a time when all UT/IC GT-treated SD mice and the majority of BMT-treated SD mice were deceased. Combination-treated SD mice analyzed at 240 days (2-fold more than the average survival and chosen as the experimental endpoint) showed only minor disease manifestations, suggestive of prolonged efficacy of the combined treatment. The increase in

Figure 5. Rescue of LAMP1 expression and GM2 storage in treated SD mice

(A) Representative western blot analyses and relative quantification showing LAMP1 protein expression in whole-brain lysate (TEL and CB) of treated mice (IC GT, BMT, and IC GT + BMT) at 120 days and 240 days and age-matched UT controls (WT, Het, and SD). Data are expressed as the mean ± SEM; n = 3–11 mice/group; one-way ANOVA followed by Kruskal-Wallis multiple comparisons test, ***p < 0.001. (B and C) Representative HPTLC and relative quantification of the aqueous phase (GM2, (B) and organic phase (GA2, (C) of total lipids obtained from whole-brain lysate (TEL and CB) of BMT- and IC GT + BMT-treated SD mice (120 days and 240 days) and age-matched UT controls (WT and SD). Quantifications are expressed as the percentage of total gangliosides (GM2) and percentage of total neutral sphingolipids (GA2). Data represent the mean ± SEM; n = 4–8 mice/group. One-way ANOVA followed by Dunnett's multiple comparison test, *p < 0.05, ***p < 0.001, ****p < 0.0001. (D) Representative IF pictures showing GM2 expression (anti-GM2 antibody, blue) and relative mask selection of immunopositive signal (black) in sagittal brain sections taken from IC GT + BMT-treated SD mice and UT controls (SD and WT) at 120 days. Magnification 10×; scale bars, 1,000 μm. (E) Correlation of Hex enzymatic activity (y axis; MUG, nanomoles per milligram per hour) and GM2 or GA2 levels (x axis, values expressed as the percentage of total gangliosides or total neutral sphingolipids, respectively) in the TEL of treated SD mice at 120 days and 240 days and age-matched UT controls (SD, WT, and Het). Each dot represents one animal. Treatment groups are shown in the legend.
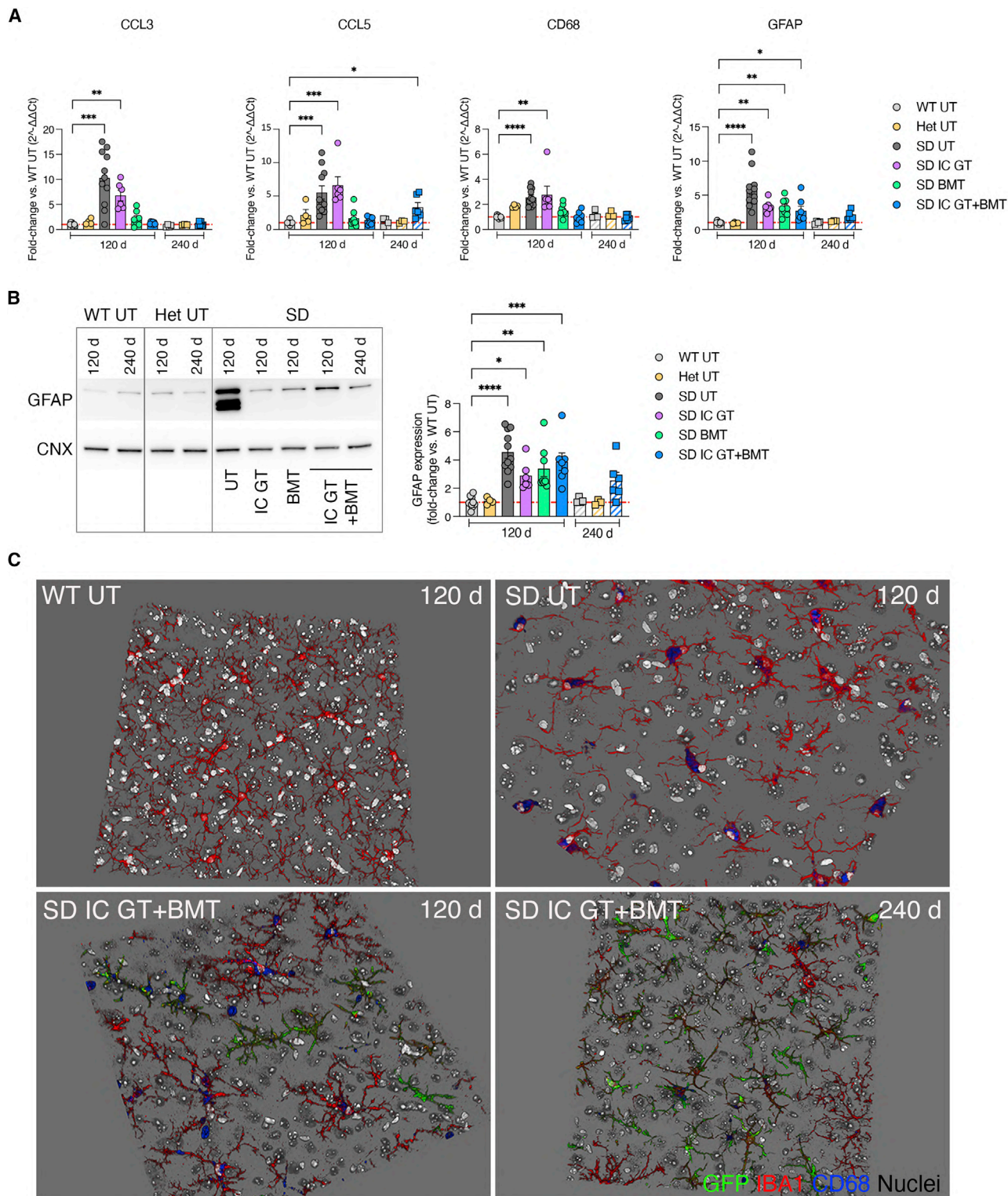
Figure 6. Reduction of neuroinflammatory markers in the CNS of treated SD mice

(A) Relative mRNA expression of neuroinflammatory cytokines (*Ccl3* and *Ccl5*), macrophage (*Cd68*), and astrocytic (*Gfap*) markers in whole-brain lysate (TEL and CB) of treated mice (IC GT, BMT, and IC GT + BMT) at 120 days and 240 days and age-matched UT controls (WT, Het, and SD). Data are expressed as fold change with respect to
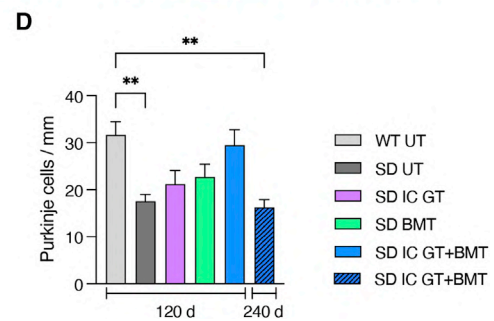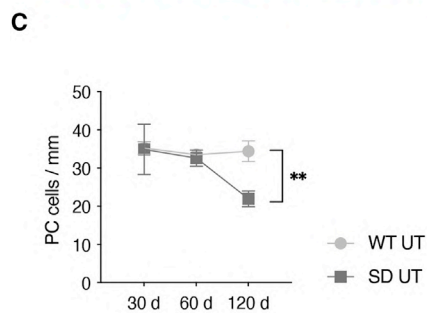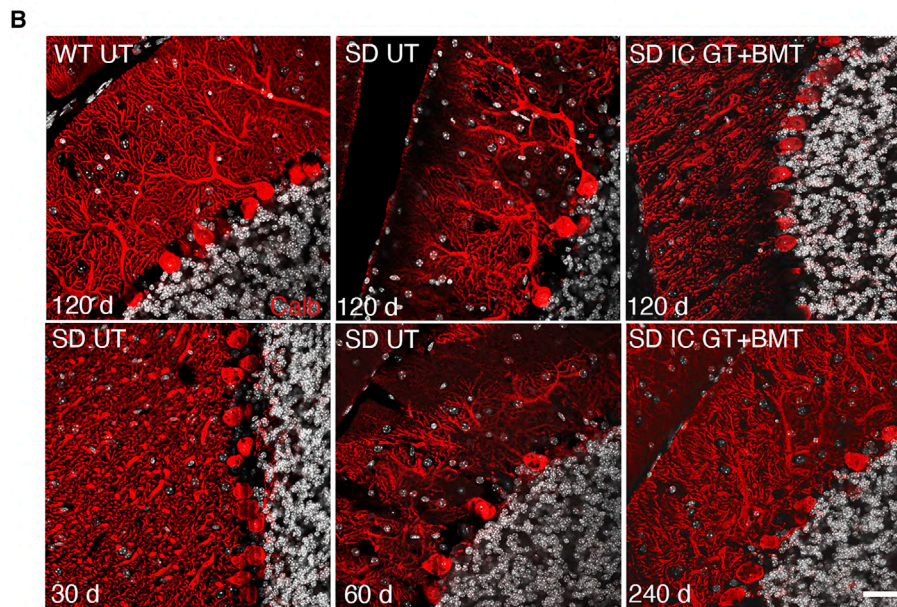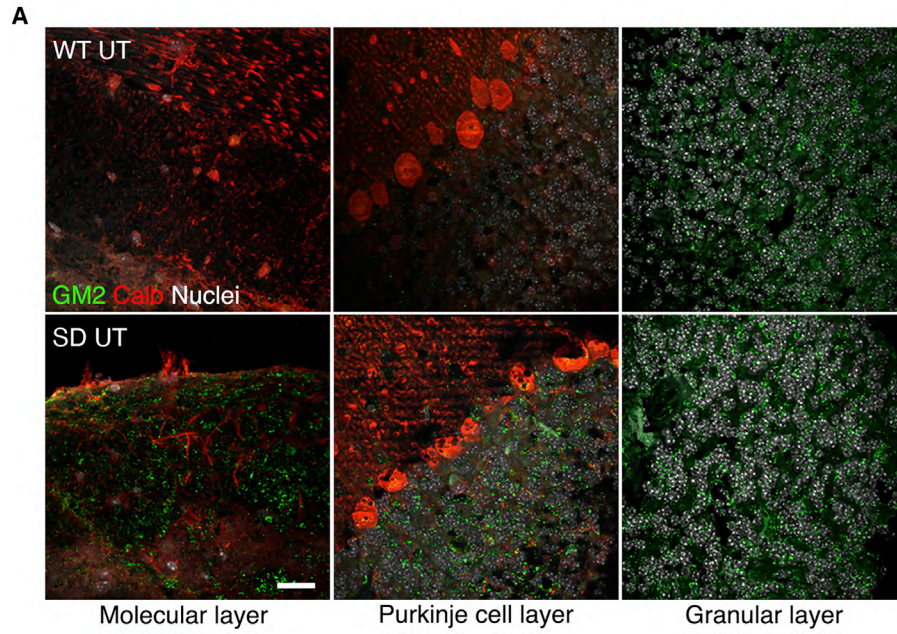
(legend continued on next page)

survival reported here for combination-treated mice was similar or lower to that reported by previous studies where the authors co-delivered two AAVs expressing the α and β subunits into the brain parenchyma[23,60,64,65] or systemically injected bicistronic AAV9 constructs.[66,67] Despite the promising pre-clinical data sustained the development of AAV GT, there are still several drawbacks associated with IC and systemic AAV delivery, including failure to correct early pathological hallmarks (e.g., myelin defects),[22,56] the neurotoxicity associated with transgene overexpression in brain cells,[28] and the potential liver and heart toxicity associated with off-target transgene expression.[66–69] These considerations, together with the known immunogenicity of AAVs,[70] dictate the need to accurately monitor individuals enrolled in first in-human AAV GT trials for GM2 gangliosidosis[27] (ClinicalTrials.gov: NCT04798235 and NCT04669535) and provide a rationale for exploring alternative/complementary therapeutic strategies.

Therapeutic improvements in GM2 gangliosidosis rely on rescue of Hex enzymatic activity to clear or counteract ganglioside storage in affected tissues, specifically in the CNS. The comparative Hex activity among different brain areas under physiological conditions has not been comprehensively investigated. The 2.5-fold higher Hex activity measured in the TEL compared with that in the CB and SC tissues of adult WT mice suggests that the enzymatic requirement is higher in the rostral versus the caudal CNS regions. The minor increase in Hex activity (7% of the normal value) in the TEL of IC GT mice and the modest amount of secretion/transport are peculiar to Hex because other lysosomal enzymes (i.e., Arylsulfatse A, ARSA and galactosylceramidase, GALC) are found throughout CNS tissue upon local intraparenchymal LV injection and supply 30%–100% of normal enzymatic activity.[32,33] Despite the modest increase, the enzyme provided by IC GT is available from a few days after neonatal injection[52] and is stable over the months before BMT and within the time frame required for full BM-derived myeloid cell engraftment in the CNS. Thus, it likely plays a key role in limiting GM2 storage buildup and delaying pathological progression. Upon BMT, donor BM-derived myeloid cells engraft into the CNS, providing additional enzyme and trophic support and reconstituting the myeloid cell population in the PNS and peripheral organs, which are not targeted by intraparenchymal LV Hex injection. Use of full myeloablation conditioning with busulfan[54] accounted for the robust and stable hematopoietic chimerism achieved in SD mice upon BMT in this study (90%–100%) compared with in previous studies, where engraftment was low or not assessed.[18,19,51,71] The analysis performed at 120 days showed complete reconstitution of enzymatic activity in the BM of SD mice that received BMT, indicative of complete repopulation of the hematopoietic compartment, and significant and sta-

ble rescue of enzymatic activity in the liver and spleen (40%–80% of the WT), indicating the presence of functional donor-derived tissue macrophages behaving as a long-term source of Hex enzyme. We observed slower kinetics for Hex activity rescue in the SN, suggesting that at least 6 months are necessary to achieve full repopulation of the PNS and peripheral organs by donor-derived cells. This slow repopulation may, in part, explain the limited efficacy of the allogeneic hematopoietic stem cell transplantation (HSCT) in rescuing the severe and progressive peripheral neuropathy associated with rapidly progressive forms of neuronopathic LSDs.[72,73]

In line with previous studies,[52,71] we found a time-dependent caudal-to-rostral distribution of donor-derived myeloid cells in the CNS tissues of BMT- and combination-treated mice. Accordingly, enzymatic reconstitution was achieved earlier in transplanted SD mice and at higher levels in the SC, with the TEL showing the lowest Hex activity with respect to physiological levels. The increase in enzymatic activity measured in combination-treated animals at 240 days of age confirmed that infiltration of donor-derived myeloid cells into the CNS is a slow and progressive process, and it supported the rationale for using combined approaches to delay or halt progression of the early-onset forms of GM2 gangliosidosis. Indeed, the progressive rescue of enzymatic activity provided by combined therapy, but not IC GT or BMT in isolation, normalized LAMP1 expression and strongly reduced GM2 and GA2 storage to levels comparable with those found in 30-day-old asymptomatic UT SD mice. Our analysis showed a clear correlation between enzymatic activity and residual ganglioside storage in the TEL, indicating that at least 20%–25% of normal enzymatic activity (measured from the total tissue lysate and CSF) is needed to ensure the 50%–70% reduction in GM2 and GA2 storage that distinguishes the therapeutic effects of combined treatments from those of single treatments. Drawing accurate conclusions regarding the similarities/differences of our combined approach versus AAV GT in terms of enzymatic rescue, GM2 storage, or neuroinflammation is complicated because of the extremely variable experimental settings of the different AAV GT studies, which often do not include simultaneous assessment of these readouts.[23,60,64,66,69,74] Still, a major indication derived from these reports is that the availability of a large supply of functional enzyme (provided it is not toxic to the recipient cells) is usually associated with enhanced therapeutic benefit. In this perspective, our results concur with previous studies showing that 30%–60% of normal Hex enzymatic activity is required for an 80%–90% reduction in GM2 storage in the CNS tissues of affected mice,[67,75] and with reasonable accuracy, they indicate the threshold of enzymatic activity that, when measured in the CSF of individuals undergoing experimental treatments, could be associated with therapeutic benefit.

---

the WT (set as 1) after normalization to *Gapdh* expression. (B) Representative western blot and relative quantification showing the expression of GFAP protein in treated mice (IC GT, BMT, and IC GT + BMT) at 120 days and 240 days and age-matched UT controls (WT, Het, and SD). Data are expressed as fold change with respect to the WT (set as 1) after normalization to calnexin (CNX) expression. Data in (A) and (B) represent the mean ± SEM; n = 3–11 animals/group. One-way ANOVA followed by Kruskal-Wallis multiple comparisons test; *p < 0.05, **p < 0.01, ***p < 0.001, ****p < 0.0001. (C) 3D projections of z stack images showing the presence of donor-derived GFP+ cells (green) and resident cells expressing Iba1 (microglia, red) and CD68 (macrophages, blue) in the TEL of IC GT + BMT-treated SD mice at 120 days and 240 days and UT controls (WT and SD). Nuclei counterstained with Hoechst, gray. Images were acquired at 40× magnification.

A

GM2 Calb Nuclei

WT UT

SD UT

Molecular layer | Purkinje cell layer | Granular layer

B

WT UT — 120 d — Calb
SD UT — 120 d
SD IC GT+BMT — 120 d
SD UT — 30 d
SD UT — 60 d
SD IC GT+BMT — 240 d

C

PC cells / mm

30 d   60 d   120 d

WT UT
SD UT

**

D

Purkinje cells / mm

120 d   240 d

WT UT
SD UT
SD IC GT
SD BMT
SD IC GT+BMT
SD IC GT+BMT

**   **

(legend on next page)

The complementary kinetics of the enzyme provided by IC GT and BMT, as well as the modality of action of these treatments, largely account for their synergy when combined. Reactive astrocytes, resident macrophages/microglia, and blood-borne immune cells are critical cellular components in mediating neuroinflammation,[76–78] which is a hallmark of different neurodegenerative disorders and has been linked to several LSDs, including GM2 gangliosidosis.[79] Our results indicate that there is an important inflammatory response in the regions of SD mouse brains where GM2 storage is more prominent. The local source of enzyme provided by IC GT is insufficient to counteract progressive neuroinflammation. In contrast, animals transplanted with BMT showed reduced expression levels of inflammation-related genes, confirming the immunomodulatory and anti-inflammatory properties of BM-derived cells engrafted into the CNS.[18,19] Long-lived combination-treated animals showed normalized inflammatory conditions and reduced astrogliosis, confirming the synergistic effect and long-lasting efficacy of the sequential treatments.

Although our results support the efficacy of combined treatments in providing a timely enzymatic supply and rescue of disease-associated hallmarks in multiple affected tissues and organs, they also highlighted some aspects of the complex SD pathology that are refractory to correction. Neuronal apoptosis and degeneration have been described in specific regions of GM2-gangliosidos animal models and affected individuals.[23,80] However, the molecular mechanisms whereby GM2 accumulation in neurons triggers neurodegeneration remain unclear. Cerebellar pathology has been described in individuals with juvenile- and late-onset TSD and SD,[81–84] in a sheep model of GM2 gangliosidosis,[85] and in a mouse model of GM2 activator deficiency,[86] but it has been poorly investigated in SD mice. We observed altered cerebellar PC morphology in symptomatic SD mice, which are clearly ataxic. Moderate hindlimb ataxia and weakness persist in long-lived combination-treated SD mice. Further investigations are warranted to understand the cause-and-effect relationships of GM2 storage and calbindin expression and localization in PCs and other cerebellar cell types involved in the neural circuits that regulate motor coordination. Combined treatments and BMT transiently counteracted PC loss without completely rescuing cell morphology and normalizing calbindin expression. Direct cerebellar injection of therapeutic vectors could be more effective to correct these pathological hallmarks.

Defects in myelin structure and composition have been described in the CNS of GM2 gangliosidosis animal models (mice, cats, dogs, and sheep)[56,58–60,87,88] and affected individuals.[61] However, it is still unclear whether the myelin defects are a consequence of neurodegeneration or whether they have a primary role in the pathogenesis, as suggested by their early occurrence in SD mice.[60] Here we showed that the progressive hypo/demyelination and infiltration of inflammatory cells into SC tissues of 120-day-old SD mice is stabilized, if not normalized, by combined IC GT and BMT treatment. These effects were not observed in the optic nerve, where extensive fiber loss was present 240 days after treatment. Indeed, all combination-treated mice became blind at around 5 months of age. This lack of benefit may be a consequence of the low enzymatic supply provided by the therapy, by the impossibility to counteract established damage, or both. Further analyses are needed to investigate the role of region-specific demyelination in disease progression, to establish whether it is a consequence of or a contributing factor to the pathological phenotype, and to discover effective strategies to counteract the phenomenon, specifically in regions that appear to be more resilient to correction. Anticipating the timing of BMT and optimizing myeloablative protocols to enhance the myeloid reconstitution of CNS tissues by donor HSCs may address and overcome these issues.

The results of this study provide proof-of-concept evidence of the feasibility and efficacy of combining LV-mediated IC GT and BMT to target the CNS, PNS, and peripheral tissues with appropriate timing to counteract rapid disease progression in a relevant murine model of GM2 gangliosidosis. Our study highlights that the short-term advantage provided by early (even if only modest) enzymatic supply in CNS tissues through IC GT enhances the long-term benefits of HC-derived myeloid progeny, which provides a reservoir of functional enzyme in all affected tissues and counteracts the detrimental neuroinflammation that current *in vivo* IC GT approaches fail to fully correct. We also identified the threshold for tissue/CSF enzymatic activity that is required to achieve a reduction in brain GM2 storage, which correlates with improved benefit, with important implications for the interpretation of current and future experimental trials. In terms of clinical translation, use of autologous hematopoietic stem cells genetically modified by LVs to express Hex enzymes[37] may overcome the current limitation of allogeneic BMT or HSCT, improving the safety and increasing the benefits of the proposed combined strategy. *Ex vivo* HSC GT has recently received fullmarketing authorization in Europe for treatment of individuals with early-onset metachromatic leukodystrophy (using autologous CD34+ cells transduced with an LV encoding the ARSA gene; Libmeldy)[89,90] and is in advanced stages of clinical testing for other neurodegenerative

Figure 7. Effect of treatments on cerebellar pathology of SD mice

(A) Representative confocal pictures showing GM2 storage in the cerebellar molecular layer, Purkinje cell (PC) layer, and granular layer of UT WT and SD mice at 120 days. GM2, green; calbindin (Calb), red; nuclei counterstained with Hoechst, white. Scale bar, 25 μm. (B) Representative confocal images showing calbindin+ PCs (red) in UT mice of different ages (WT, 120 days; SD, 30 days, 60 days, and 120 days) and IC GT + BMT-treated SD mice at 120 days and 240 days. Calbindin, red. Nuclei counterstained with Hoechst, gray. Scale bar, 50 μm. (C) Quantification of the number of PCs in UT SD and WT mice at 30 days, 60 days, and 120 days. Data represent the number of PCs per millimeter and are expressed as the mean ± SEM; n = 1–10 mice/group. two-way ANOVA followed by Bonferroni's multiple comparisons test; **p < 0.01. (D) Quantification of the number of PCs in treated mice (IC GT, BMT, and IC GT + BMT) at 120 days and 240 days and age-matched UT controls (WT and SD). Data represent the number of PCs per millimeter in all cerebellar lobules of each brain section (3–4 sagittal sections per mouse). Data are expressed as mean ± SEM; n = 4–6 mice/group; one-way ANOVA followed by Kruskal-Wallis multiple comparisons test, **p < 0.01.
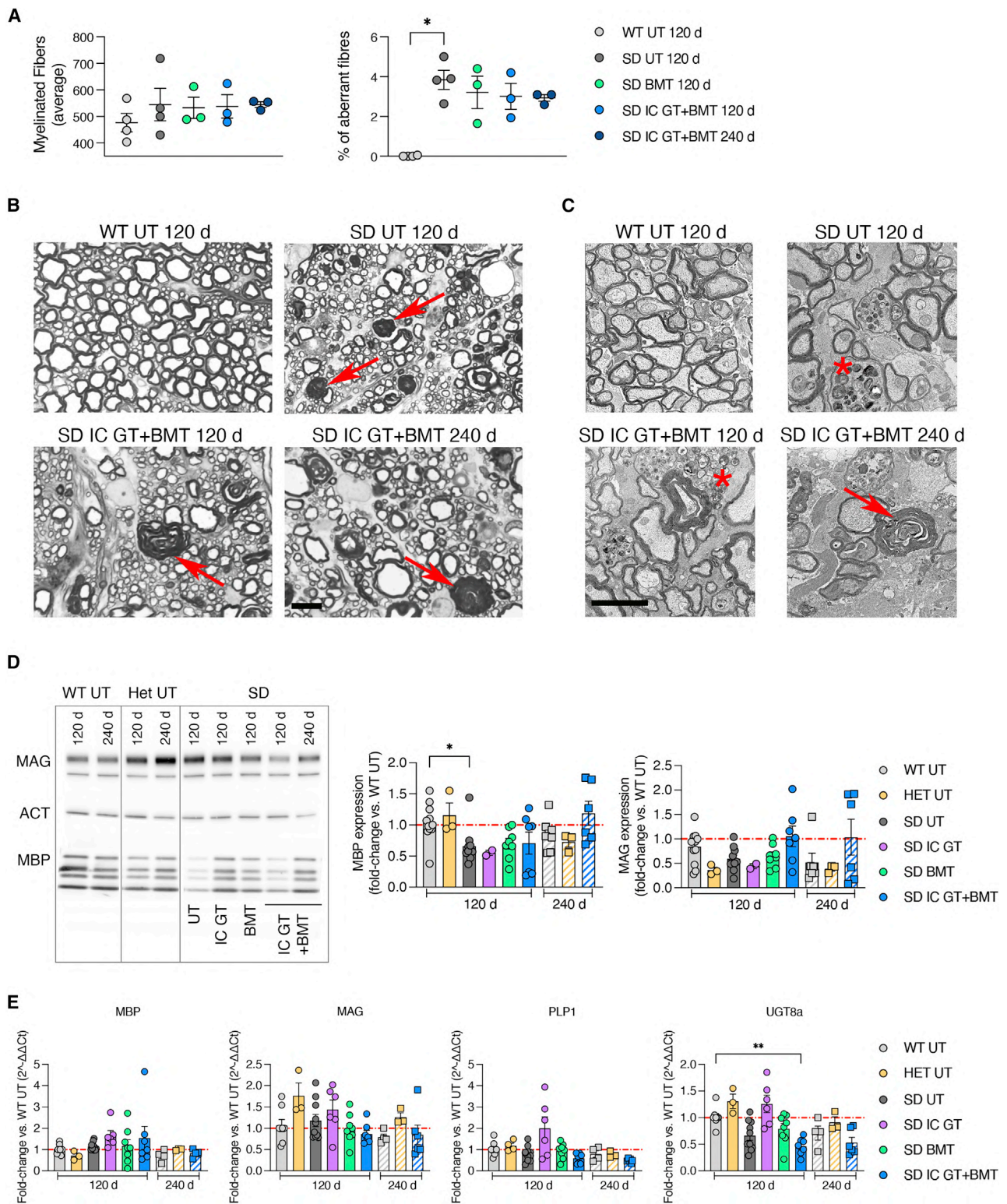
Figure 8. Analyses of the myelin compartment in treated SD mice

(A) Quantification of myelinated fibers and percentage of demyelinated/degenerated (aberrant) fibers among total fibers in SC sections from treated mice (IC GT, BMT, and IC GT + BMT) at 120 days and 240 days and age-matched UT controls (WT and SD). Data are expressed as mean ± SEM; n = 3–4 mice/group; nonparametric one-way ANOVA

(legend continued on next page)

LSDs.[73,91] Optimization of combined LV-mediated *in vivo* and *ex vivo* GT protocols could address the unmet medical needs of individuals with GM2 gangliosidoses and potentially other LSDs for which therapeutic options are absent or insufficient.

MATERIALS AND METHODS

Animals
SD mice (*hexb*^{−/−}) were generated as described previously.[17] Mice were bred via heterozygosis, and *Hexb*^{+/+} and *hexb*^{+/−} littermates were used as controls. CAG GFP transgenic mice (C57BL/6-Tg (CAG-EGFP)1Osb/J) were purchased from The Jackson Laboratory (Bar Harbor, ME USA). CAG GFP mice have an EGFP cDNA under control of a chicken β-actin promoter and cytomegalovirus enhancer (CAG) and show widespread EGFP fluorescence. Mouse colonies were maintained in the animal facility at the San Raffaele Scientific Institute (Milan, Italy).

LVs
We used monocistronic third-generation LVs expressing cDNA encoding murine hexa or murine hexb (LV.hexA or LV.hexB, respectively) or GFP cDNA (LV.GFP) under control of the human PGK promoter. LVs were cloned, produced, and titrated as described previously:[37]

- LV.hexA: titer, 0.68×10^9 TU/mL; infectivity, 3.78×10^4 TU/ng;
- LV.hexB: titer, 1.15×10^9 TU/mL; infectivity, 7.47×10^4 TU/ng;
- LV.GFP: titer, 1.1×10^{10} TU/mL; infectivity, 1.5×10^5 TU/ng.

Treatments
IC GT
SD mice and controls were injected with LV preparations at 2 days. Pups were anesthetized in crushed ice and placed on a refrigerated stage. LVs (4×10^6 TU/μL) were injected bilaterally into the EC under stereotactic guidance using a syringe (33G, model 1701 RN Neuros, 65460-05, 10 μL; Hamilton, Reno, NV, USA). Stereotactic coordinates were as follows (millimeters from the frontal cerebral vein): Anteroposterior (AP), +1; Mediolateral (ML), +2; Dorsoventral (DV), −1. After injection, the pups were placed on a heating pad, monitored for 15 min, and then placed in their cage with their mother.

BMT
Total BM was flushed from the tibiae, femora, and humeri of 4- to 8-week-old tgGFP mice as described previously.[52] One tgGFP mouse served as a donor for six recipient mice. Cells were suspended in PBS (5×10^6 cells/200 μL) and immediately injected into the tail vein of 60-day-old busulfan-conditioned SD mice (125 mg/kg for 4 days)[92]. Survival after the procedure was 100%. Part of the BM suspension was collected for enzymatic and cytofluorimetric activity, and 100% of BM cells isolated from the tgGFP mice were GFP+ and expressed physiological levels of β-hex activity.

Combined treatment
60-day-old mice that had been treated with IC GT on post-natal day 2 (P2) received BMT the day after completion of the myeloablation protocol by intraperitoneal (i.p.) busulfan injection (125 mg/kg for 4 days). Mice dying within 2–3 weeks after busulfan conditioning were excluded from subsequent analyses. Animals were euthanized at 120 days of age (average lifespan of UT SD mice), 240 days of age (chosen as endpoint of the study), or when they reached the human disease endpoint (weight loss >80% with respect to age-matched WT mice or inability to eat and drink). UT SD, Het, and WT littermates were included as controls.

Tissue collection and processing
Mice were euthanized after anesthetic agent overdose (ketamine/xylazine) via intracardiac perfusion of the descending aorta with 0.9% NaCl. Brain hemispheres were separated, and one hemisphere was cut to separate the TEL from the CB; the tissues were immediately frozen and used to measure enzymatic activity.[93] The other hemisphere was cut into two equal sagittal slices; one was post-fixed in 4% paraformaldehyde (PFA) in PBS and used for IF, and the other was smashed through a cell strainer in PBS, washed, pelleted, and quickly frozen for later biochemical and molecular assays (thin-layer chromatography and RNA and protein extraction). Whole SC was collected and sagittally halved, and the SN, spleen, and liver were isolated and split in half. For each of these tissues, one half was quickly frozen in liquid nitrogen for enzymatic activity analysis, and the other half was post-fixed in 4% PFA in PBS for IF analysis. Total BM was flushed from tibiae, femora, and humeri and collected for enzymatic activity and cytofluorimetric analyses. We collected the CSF from the *cisterna magna* immediately prior to euthanasia using a glass capillary (only in mice at 120 days).

IF
Free-floating vibratome sections (40 μm thick) were incubated with blocking solution (10% normal goat serum [NGS] + 0.3% Triton

followed by Dunn's multiple comparisons test, *p < 0.05. (B) Semithin section analysis of lumbar SC of IC GT + BMT-treated SD mice at 120 days and 240 days and UT controls (WT and SD). Red arrows indicate aberrant myelin. Scale bar, 10 μm. (C) Electron microscopy images of optic nerves in treated SD and UT controls at 120 days and 240 days. Red arrows indicate aberrant myelin, and asterisks mark macrophages. Scale bar, 2 μm. (D) Representative western blot analyses and relative quantification showing MBP and MAG protein expression in whole-brain lysate (TEL and CB) of treated mice (IC GT, BMT, and IC GT + BMT) at 120 days and 240 days and age-matched UT controls (WT, Het, and SD). Data are expressed as fold change with respect to the WT (set as 1) after normalization to β-actin expression. Data represent the mean ± SEM; n = 3–10 mice/group. One-way ANOVA followed by Kruskal-Wallis multiple comparisons test, *p < 0.05. (E) Expression of myelin-related genes (*Mbp*, *Mag*, *Plp1*, and *Ugt8a*) in whole-brain lysate (TEL and CB) of treated mice (IC GT, BMT, and IC GT + BMT) at 120 days and 240 days and age-matched UT controls (WT, Het, and SD). Data are expressed as fold change with respect to the WT (set as 1) after normalization to Gapdh. Data represent the mean ± SEM; n = 2–12 mice/group. One-way ANOVA followed by Kruskal-Wallis multiple comparisons test, **p < 0.01. No significant differences are found between UT SD and UT WT mice or between SD-treated mice and SD UT counterparts.

X-100 in PBS) for 1 h at room temperature (RT) and then incubated overnight at 4°C with primary antibody diluted in blocking solution. After three thorough washes of 5 min each, species-specific fluorophore-conjugated secondary antibodies diluted in 10% NGS in PBS were added. Tissue sections were counterstained with Hoechst 33342, Trihydrochloride, Trihydrate (Thermo Fisher Scientific, Waltham, MA, USA) for nuclei, washed in 1× PBS, collected, and mounted on glass slides using Fluorsave (Calbiochem, San Diego, CA, USA).

The following primary antibodies were used: chicken anti-GFP (1:500, ab-13970, Abcam, Cambridge, UK), glial fibrillary acidic protein (polyclonal, 1:1,000, ZO334, Dako-Agilent, Santa Clara, CA, USA; monoclonal, 1:1,000, MAB 3402, Millipore, Burlington, MA, USA), rabbit anti Iba1 (1:100, 019-19741, Wako Pure Chemicals Industries, Neuss, Germany), rat anti CD68 (1:200, clone FA-11/MCA1957, Bio-Rad, Hercules, CA, USA), rabbit anti LAMP1 (1:200, AB24170; Abcam), rat anti-LAMP1 hybridoma (1:300, 1D4B, Developmental Studies Hybridoma Bank at The University of Iowa), mouse anti-GM2 (1:500, A2576, TCI Europe), and rabbit anti-Calbindin (1:1,000, CB-38A, Swant, Burgdorf, Switzerland).

The secondary antibodies were from Thermo Fisher Scientific : Alexa 488 (1:1,000, anti-rabbit A11008, anti-mouse A11001, and anti-chicken A11039), Alexa 546 (1:2,000, anti-mouse A11039 and anti-rabbit A11010), and Alexa 633 (1:500, anti-rat A21094 and anti-mouse A21050).

Image acquisition

Confocal images were acquired at different magnifications with a TCS SP8 confocal microscope (Leica, Wetzlar, Germany) or an RS-G4 upright confocal microscope (MAVIG Research, Munich, Germany). Data were analyzed with Fiji software (ImageJ, National Institutes of Health, Bethesda, MD, USA),[94] LasX software (Leica Application Suite X, RRID: SCR_013673), and Imaris viewer software (Oxford Instruments, Abingdon-on-Thames, UK). Images were imported into Adobe Photoshop 2021 for brightness and contrast adjustments and to merge the channels.

Quantification of PC number

Confocal images were acquired at 20× magnification using a MAVIG RS-G4 upright confocal microscope. We counted the number of PCs in the lobules of each section (3–4 sagittal sections per mouse) and related this value to the length of the relevant PC layer, as measured in micrometers using Fiji software.[94]

Cytofluorimetric analyses of PB and BM samples

PB was collected from BMT-treated mice and UT controls, and 20 mL of each sample was incubated for 30 min at 4°C with rat anti-mouse CD45-VioBlue (Miltenyi Biotec, Bergisch Gladbach, Germany; catalog number 130-110-802) and then for 15 min with ammonium-chloride-potassium (ACK) buffer for RBC lysis. Samples were centrifuged and suspended in fluorescence-activated cell sorting (FACS) buffer (PBS + 5% fetal bovine serum [FBS] + 1% BSA). Then the cells

were analyzed for CD45 and GFP positivity using a flow cytometer (Canto II, BD Biosciences, Franklin Lakes, NJ, USA), and the data were analyzed using the FlowJo software (Ashland, OR, USA). The remaining PB sample aliquots were analyzed using an automated hemocytometer (ProCyte Dx Hematology Analyzer, IDEXX Laboratories, Westbrook, ME, USA) to determine the complete blood count variables.

BM samples from donor and recipient mice were resuspended in FACS buffer for 15 min and stained with CD45-BV510 (BD Biosciences, catalog number 563891), CD11b-APC (BD Biosciences, catalog number 553312), CD19-phycoerytrin (PE; BioLegend, San Diego, CA, USA; catalog number 152407), and CD3-fluorescein isothiocyanate (FITC; BioLegend, catalog number 100203) for 20 min; the GFP signal was measured by direct fluorescence. After washing in PBS, pellets were resuspended in 300 μL of PBS. Cells were analyzed by flow cytometry using a Canto instrument (Canto II, BD Biosciences). All data were analyzed using the FlowJo software.phycoerytrin

Morphological analysis of the SC and optic nerve

Semithin section analysis of SCs was performed as reported previously.[95,96] To perform morphometric analysis, digitalized images of SC cross-sections were obtained from similar regions (cervical and lumbar) with a 100× objective and Leica DFC300F digital camera. At least 10 images per animal were analyzed with QWin software (Leica Microsystems), and the total number of fibers, number of fibers displaying myelin degeneration, and axon diameter distribution were calculated. Ultrastructural analysis was performed on optic nerves with 20–40 images per animal, which were acquired using the TALOS L120C transmission electron microscope (Thermo Fisher Scientific).

Determination of Hex activity and isoenzyme composition

The β-Hex activity and chromatographic profiles were measured as described previously.[37] Briefly, hexosaminidase activity was determined using MUG and MUGS substrates dissolved in 0.1 M citrate/0.2 M disodium phosphate buffer (pH 4.5). The enzymatic reactions were performed using 50 μL of test sample incubated with 100 μL of substrate at 37°C. All reactions were stopped by adding 2.850 mL of 0.2 M glycine/NaOH (pH 10.6). The fluorescence of the liberated 4-methylumbelliferone was measured on an LS50B spectrofluorometer (PerkinElmer, Waltham, MA; λ excitation, 360 nm; λ emission, 446 nm).

Gene expression analyses

Total RNA from CNS tissues was extracted using RNeasy Lipid Tissue with Qiazol (QIAGEN, Hilden, Germany) in accordance with the manufacturer's protocol. The quantity of RNA was determined using a 260/280-nm optical density (OD) reading on an ND-1000 spectrophotometer (NanoDrop, Pero, Italy). mRNA reverse transcription was performed using the QuantiTect reverse transcription kit (QIAGEN) in accordance with the manufacturer's protocol. qPCR was performed in Optical 96-well Fast Thermal Cycling Plates on Viia7

(Thermo Fisher Scientific) using the following thermal cycling conditions: 1 cycle at 95°C for 5 min and 40 cycles at 95°C for 15 s and 60°C for 1 m, using Universal PCR Master Mix and TaqMan Gene Expression Assays (Thermo Fisher Scientific). SDS 2.2.1 software was used to extract raw data. The relative expression of mRNA for the target genes was calculated using the $2-\Delta\Delta Ct$ method.

Commercial probes and primers (Thermo Fisher Scientific) were as follows: *Gapdh* (glyceraldehyde 3-phosphate dehydrogenase), Mm99999915_g1; *Cd68*, Mm03047343_m1; *Ccl3*, Mm00441259_g1; *Ccl5*, Mm01302427_m1; *Gfap*, Mm01253033_m1; *Mbp*, Mm0126 6402_m1; *Mag*, Mm00487538_m1; *Plp1*, Mm00456892_m1; and *Ugt8a*, Mm00495930_m1.

Western blot analyses
Protein content was determined through a DC protein assay (Bio-Rad) following the manufacturer's protocol. After boiling for 5 min in sample buffer, samples containing 5–20 μg of protein were separated on 4%–12% acrylamide gel SDS-PAGE electrophoresis before antigen detection with the primary and secondary antibodies listed below. Immunodetection was performed using the Amersham ECL Plus kit (GE Healthcare, Little Chalfont, Buckinghamshire, UK). Primary antibodies were as follows: rabbit anti-LAMP1 (1:100, AB24170, Abcam), rabbit anti-GFAP (1:100,000, ZO334, Dako), mouse anti-MBP (1:4,000, clone SMI 94/SMI 99, BioLegend), rabbit anti-MAG (1:1,000, 34-6200, Thermo Fisher Scientific), rabbit anti-calnexin (1:5,000, C4731, Sigma-Aldrich, St. Louis, MO, USA), and mouse anti-actin (1:10,000; sc-1616r, Santa Cruz Biotechnology, Dallas, TX, USA). Secondary antibodies (Chemicon, Temecula, CA, USA) were as follows: goat anti-rabbit horseradish peroxidase (HRP) (1:10,000, AP132P) and goat anti-mouse HRP (1:10,000, AP124P).

Thin-layer chromatography
Lipids associated with the total cell lysates were extracted twice with chloroform/methanol 2:1 (v/v) and chloroform/methanol/water 20:10:1 (v/v). Total lipid extracts were subjected to phase separation according to the Folch method with some modifications. Finally, the organic phases were subjected to alkaline methanolysis to remove glycerophospholipids.[97,98] Lipids contained in the organic- and aqueous-phase fractions corresponding to the same amount of cell proteins were separated by high-pressure thin-layer chromatography (HPTLC) using the solvent system chloroform:methanol:water 110:40:6 (v/v/v) and chloroform:methanol:$CaCl_2$ 0.2%, 50:42:11 (v/v/v), respectively. Gangliosides were visualized by Ehrlich reagents, whereas the lipids contained in the organic phase were observed using anisaldehyde staining. Lipid bands were detected by digital acquisition and quantified using ImageJ software. After separation, the lipids were identified by co-migration with authentic lipid standards.

Statistics
Data were analyzed with GraphPad Prism version 8.0 for Macintosh (GraphPad, San Diego, CA, USA) and expressed as the mean ± standard error of the mean (SEM). Unpaired Student's t test and one-way or two-way ANOVA followed by post-tests were used when appropriate (statistical significance: $p < 0.05$). Survival curves were analyzed with log rank (Mantel-Cox) test. The number of samples and statistical tests used are indicated in the figure legends.

Study approval
All experiments and procedures described in this study were conducted under an approved protocol of the Institutional Committee for the Good Animal Experimentation of the San Raffaele Scientific Institute and were reported to the Ministry of Health as required by Italian law (Institutional Animal Care and Use Committee - IACUC #791 and #1145).

AUTHOR CONTRIBUTIONS
D.S. and F.O. conducted experiments and acquired and analyzed data. F.M., C.A., and S.M. performed and analyzed enzymatic activity assays and DEAE chromatography. V.A., R.D.G., and A.B. performed and analyzed morphometric and ultrastructural analyses on CNS and PNS tissues. M.V. and M.A. performed and analyzed TLC to assess ganglioside content. A.B., S.M., F.M., and M.A. provided reagents, intellectual input, and critical review of the manuscript. D.S., F.O., and A.G. designed the study, analyzed data, and wrote the manuscript.

DECLARATION OF INTERESTS
The authors declare no competing interests.

REFERENCES
1. Regier, D.S., Proia, R.L., D'Azzo, A., and Tifft, C.J. (2016). The GM1 and GM2 gangliosidoses: natural history and progress toward therapy. Pediatr. Endocrinol. Rev. *13*, 663–673.

2. Mahuran, D.J. (1999). Biochemical consequences of mutations causing the GM2 gangliosidoses. Biochim. Biophys. Acta *1455*, 105–138.

3. Cordeiro, P., Hechtman, P., and Kaplan, F. (2000). The GM2 gangliosidoses databases: allelic variation at the HEXA, HEXB, and GM2A gene loci. Genet. Med. *2*, 319–327.

4. Bley, A.E., Giannikopoulos, O.A., Hayden, D., Kubilus, K., Tifft, C.J., and Eichler, F.S. (2011). Natural history of infantile G(M2) gangliosidosis. Pediatrics *128*, e1233–e1241.

5. Tsuji, D., Akeboshi, H., Matsuoka, K., Yasuoka, H., Miyasaki, E., Kasahara, Y., Kawashima, I., Chiba, Y., Jigami, Y., Taki, T., et al. (2011). Highly phosphomannosylated enzyme replacement therapy for GM2 gangliosidosis. Ann. Neurol. *69*, 691–701.

6. Matsuoka, K., Tamura, T., Tsuji, D., Dohzono, Y., Kitakaze, K., Ohno, K., Saito, S., Sakuraba, H., and Itoh, K. (2011). Therapeutic potential of intracerebroventricular replacement of modified human β-hexosaminidase B for GM2 gangliosidosis. Mol. Ther. *19*, 1017–1024.

7. Baek, R.C., Kasperzyk, J.L., Platt, F.M., and Seyfried, T.N. (2008). N-butyldeoxygalactonojirimycin reduces brain ganglioside and GM2 content in neonatal Sandhoff disease mice. Neurochem. Int. *52*, 1125–1133.

8. Andersson, U., Smith, D., Jeyakumar, M., Butters, T.D., Borja, M.C., Dwek, R.A., and Platt, F.M. (2004). Improved outcome of N-butyldeoxygalactonojirimycin-mediated substrate reduction therapy in a mouse model of Sandhoff disease. Neurobiol. Dis. *16*, 506–515.

9. Maegawa, G.H.B., Tropak, M., Buttner, J., Stockley, T., Kok, F., Clarke, J.T.R., and Mahuran, D.J. (2007). Pyrimethamine as a potential pharmacological chaperone for late-onset forms of GM2 gangliosidosis. J. Biol. Chem. *282*, 9150–9161.

10. Maegawa, G.H.B., Banwell, B.L., Blaser, S., Sorge, G., Toplak, M., Ackerley, C., Hawkins, C., Hayes, J., and Clarke, J.T.R. (2009). Substrate reduction therapy in juvenile GM2 gangliosidosis. Mol. Genet. Metab. *98*, 215–224.

11. Tallaksen, C.M.E., and Berg, J.E. (2009). Miglustat therapy in juvenile Sandhoff disease. J. Inherit. Metab. Dis. *32*, S289–S293.

12. Masciullo, M., Santoro, M., Modoni, A., Ricci, E., Guitton, J., Tonali, P., and Silvestri, G. (2010). Substrate reduction therapy with miglustat in chronic GM2 gangliosidosis type Sandhoff: results of a 3-year follow-up. J. Inherit. Metab. Dis. *33*, S355–S361.

13. Wortmann, S.B., Lefeber, D.J., Dekomien, G., Willemsen, M.A.A.P., Wevers, R.A., and Morava, E. (2009). Substrate deprivation therapy in juvenile Sandhoff disease. J. Inherit. Metab. Dis. *32*, S307–S311.

14. Clarke, J.T.R., Mahuran, D.J., Sathe, S., Kolodny, E.H., Rigat, B.A., Raiman, J.A., and Tropak, M.B. (2011). An open-label Phase I/II clinical trial of pyrimethamine for the treatment of patients affected with chronic GM2 gangliosidosis (Tay-Sachs or Sandhoff variants). Mol. Genet. Metab. *102*, 6–12.

15. von Specht, B.U., Geiger, B., Arnon, R., Passwell, J., Keren, G., Goldman, B., and Padeh, B. (1979). Enzyme replacement in Tay-Sachs disease. Neurology *29*, 848–854.

16. Shapiro, B.E., Pastores, G.M., Gianutsos, J., Luzy, C., and Kolodny, E.H. (2009). Miglustat in late-onset Tay-Sachs disease: a 12-month, randomized, controlled clinical study with 24 months of extended treatment. Genet. Med. *11*, 425–433.

17. Sango, K., Yamanaka, S., Hoffmann, A., Okuda, Y., Grinberg, A., Westphal, H., McDonald, M.P., Crawley, J.N., Sandhoff, K., Suzuki, K., et al. (1995). Mouse models of Tay-Sachs and Sandhoff diseases differ in neurologic phenotype and ganglioside metabolism. Nat. Genet. *11*, 170–176.

18. Norflus, F., Tifft, C.J., McDonald, M.P., Goldstein, G., Crawley, J.N., Hoffmann, A., Sandhoff, K., Suzuki, K., and Proia, R.L. (1998). Bone marrow transplantation prolongs life span and ameliorates neurologic manifestations in Sandhoff disease mice. J. Clin. Invest. *101*, 1881–1888.

19. Wada, R., Tifft, C.J., and Proia, R.L. (2000). Microglial activation precedes acute neurodegeneration in Sandhoff disease and is suppressed by bone marrow transplantation. Proc. Natl. Acad. Sci. U S A *97*, 10954–10959.

20. Hoogerbrugge, P.M., Brouwer, O.F., Bordigoni, P., Ringden, O., Kapaun, P., Ortega, J.J., O'Meara, A., Cornu, G., Souillet, G., Frappaz, D., et al. (1995). Allogeneic bone marrow transplantation for lysosomal storage diseases. The European Group for Bone Marrow Transplantation. Lancet *345*, 1398–1402.

21. Jacobs, J.F., Willemsen, M.A., Groot-Loonen, J.J., Wevers, R.A., and Hoogerbrugge, P.M. (2005). Allogeneic BMT followed by substrate reduction therapy in a child with subacute Tay-Sachs disease. Bone Marrow Transpl. *36*, 925–926.

22. Cachon-Gonzalez, M.B., Wang, S.Z., Ziegler, R., Cheng, S.H., and Cox, T.M. (2014). Reversibility of neuropathology in Tay-Sachs-related diseases. Hum. Mol. Genet. *23*, 730–748.

23. Sargeant, T.J., Wang, S., Bradley, J., Smith, N.J., Raha, A.A., McNair, R., Ziegler, R.J., Cheng, S.H., Cox, T.M., and Cachon-Gonzalez, M.B. (2011). Adeno-associated virus-mediated expression of beta-hexosaminidase prevents neuronal loss in the Sandhoff mouse brain. Hum. Mol. Genet. *20*, 4371–4380.

24. McCurdy, V.J., Rockwell, H.E., Arthur, J.R., Bradbury, A.M., Johnson, A.K., Randle, A.N., Brunson, B.L., Hwang, M., Gray-Edwards, H.L., Morrison, N.E., et al. (2015). Widespread correction of central nervous system disease after intracranial gene therapy in a feline model of Sandhoff disease. Gene Ther. *22*, 181–189.

25. Rockwell, H.E., McCurdy, V.J., Eaton, S.C., Wilson, D.U., Johnson, A.K., Randle, A.N., Bradbury, A.M., Gray-Edwards, H.L., Baker, H.J., Hudson, J.A., et al. (2015). AAV-mediated gene delivery in a feline model of Sandhoff disease corrects lysosomal storage in the central nervous system. ASN Neuro. *7*, 1759091415569908.

26. Bradbury, A.M., Gray-Edwards, H.L., Shirley, J.L., McCurdy, V.J., Colaco, A.N., Randle, A.N., Christopherson, P.W., Bird, A.C., Johnson, A.K., Wilson, D.U., et al. (2015). Biomarkers for disease progression and AAV therapeutic efficacy in feline Sandhoff disease. Exp. Neurol. *263*, 102–112.

27. Flotte, T., et al. (2022). AAV gene therapy for Tay-Sachs disease. Nature Medicine *28*, 251–259. https://doi.org/10.1038/s41591-021-01664-4.

28. Golebiowski, D., van der Bom, I.M.J., Kwon, C.-S., Miller, A.D., Petrosky, K., Bradbury, A.M., Maitland, S., Kühn, A.L., Bishop, N., Curran, E., et al. (2017). Direct intracranial injection of AAVrh8 encoding monkey β-N-acetylhexosaminidase causes neurotoxicity in the primate brain. Hum. Gene Ther. *28*, 510–522.

29. Mingozzi, F., and High, K.A. (2011). Immune responses to AAV in clinical trials. Curr. Gene Ther. *11*, 321–330.

30. Bradbury, A.M., Cochran, J.N., McCurdy, V.J., Johnson, A.K., Brunson, B.L., Gray-Edwards, H., Leroy, S.G., Hwang, M., Randle, A.N., Jackson, L.S., et al. (2013). Therapeutic response in feline sandhoff disease despite immunity to intracranial gene therapy. Mol. Ther. *21*, 1306–1315.

31. Hordeaux, J., Buza, E.L., Dyer, C., Goode, T., Mitchell, T.W., Richman, L., Denton, N., Hinderer, C., Katz, N., Schmid, R., et al. (2020). Adeno-associated virus-induced dorsal root ganglion pathology. Hum. Gene Ther. *31*, 808–818.

32. Lattanzi, A., Neri, M., Maderna, C., di Girolamo, I., Martino, S., Orlacchio, A., Amendola, M., Naldini, L., and Gritti, A. (2010). Widespread enzymatic correction of CNS tissues by a single intracerebral injection of therapeutic lentiviral vector in leukodystrophy mouse models. Hum. Mol. Genet. *19*, 2208–2227.

33. Lattanzi, A., Salvagno, C., Maderna, C., Benedicenti, F., Morena, F., Kulik, W., Naldini, L., Montini, E., Martino, S., and Gritti, A. (2014). Therapeutic benefit of lentiviral-mediated neonatal intracerebral gene therapy in a mouse model of globoid cell leukodystrophy. Hum. Mol. Genet. *23*, 3250–3268.

34. Palfi, S., Gurruchaga, J.M., Ralph, G.S., Lepetit, H., Lavisse, S., Buttery, P.C., Watts, C., Miskin, J., Kelleher, M., Deeley, S., et al. (2014). Long-term safety and tolerability of ProSavin, a lentiviral vector-based gene therapy for Parkinson's disease: a dose escalation, open-label, phase 1/2 trial. Lancet *383*, 1138–1146.

35. Palfi, S., Gurruchaga, J.M., Lepetit, H., Howard, K., Ralph, G.S., Mason, S., Gouello, G., Domenech, P., Buttery, P.C., Hantraye, P., et al. (2018). Long-term follow-up of a phase I/II study of ProSavin, a lentiviral vector gene therapy for Parkinson's disease. Hum. Gene Ther. Clin. Dev. *29*, 148–155.

36. Meneghini, V., Lattanzi, A., Tiradani, L., Bravo, G., Morena, F., Sanvito, F., Calabria, A., Bringas, J., Fisher-Perkins, J.M., Dufour, J.P., et al. (2016). Pervasive supply of therapeutic lysosomal enzymes in the CNS of normal and Krabbe-affected non-human primates by intracerebral lentiviral gene therapy. EMBO Mol. Med. *8*, 489–510.

37. Ornaghi, F., Sala, D., Tedeschi, F., Maffia, M.C., Bazzucchi, M., Morena, F., Valsecchi, M., Aureli, M., Martino, S., and Gritti, A. (2020). Novel bicistronic lentiviral vectors correct β-Hexosaminidase deficiency in neural and hematopoietic stem cells and progeny: implications for in vivo and ex vivo gene therapy of GM2 gangliosidosis. Neurobiol. Dis. *134*, 104667.

38. Ogawa, Y., Sasanuma, Y., Shitara, S., Koshizuka, A., Okada, R., Sakuraba, H., and Oishi, K. (2019). Abnormal organization during neurodevelopment in a mouse model of Sandhoff disease. Neurosci. Res. *155*, 12–19.

39. Ogawa, Y., Kaizu, K., Yanagi, Y., Takada, S., Sakuraba, H., and Oishi, K. (2017). Abnormal differentiation of Sandhoff disease model mouse-derived multipotent stem cells toward a neural lineage. PLoS One 12, e0178978.

40. Higami, S., Nishizawa, K., Omura, K., Sugimoto, K., and Isshiki, G. (1976). Prenatal diagnosis and fetal pathology of Tay-Sachs disease. Tohoku J. Exp. Med. 118, 323–330.

41. Omura, K., Higami, S., Issiki, G., Nishizawa, K., and Tada, K. (1973). Prenatal diagnosis of the Hurler syndrome: mucopolysaccharide pattern in amniotic fluid. Tohoku J. Exp. Med. 111, 87–91.

42. Higami, S., Omura, K., Nishizawa, K., Yamashita, T., and Tada, K. (1978). Prenatal diagnosis and fetal pathology of Niemann-Pick disease. Tohoku J. Exp. Med. 125, 11–17.

43. Igisu, H., and Suzuki, K. (1984). Progressive accumulation of toxic metabolite in a genetic leukodystrophy. Science 224, 753–755.

44. Santambrogio, S., Ricca, A., Maderna, C., Ieraci, A., Aureli, M., Sonnino, S., Kulik, W., Aimar, P., Bonfanti, L., Martino, S., et al. (2012). The galactocerebrosidase enzyme contributes to maintain a functional neurogenic niche during early post-natal CNS development. Hum. Mol. Genet. 21, 4732–4750.

45. Patil, S.A., Hb Maegawa, G., and Maegawa, G.H. (2013). Developing therapeutic approaches for metachromatic leukodystrophy. Drug Des. Devel. Ther. 7, 729–745.

46. Sandhoff, K., and Harzer, K. (2013). Gangliosides and gangliosidoses: principles of molecular and metabolic pathogenesis. J. Neurosci. 33, 10195–10208.

47. Ogawa, Y., Irisa, M., Sano, T., Yanagi, Y., Furusawa, E., Saito, T., Yamanaka, S., Itoh, K., Sakuraba, H., and Oishi, K. (2018). Improvement in dysmyelination by the inhibition of microglial activation in a mouse model of Sandhoff disease. Neuroreport 29, 962–967.

48. Hasegawa, D., Tamura, S., Nakamoto, Y., Matsuki, N., Takahashi, K., Fujita, M., Uchida, K., and Yamato, O. (2013). Magnetic resonance findings of the corpus callosum in canine and feline lysosomal storage diseases. PLoS One 8, e83455.

49. Arthur, J.R., Lee, J.P., Snyder, E.Y., and Seyfried, T.N. (2012). Therapeutic effects of stem cells and substrate reduction in juvenile Sandhoff mice. Neurochem. Res. 37, 1335–1343.

50. Lee, J.P., Jeyakumar, M., Gonzalez, R., Takahashi, H., Lee, P.J., Baek, R.C., Clark, D., Rose, H., Fu, G., Clarke, J., et al. (2007). Stem cells act through multiple mechanisms to benefit mice with neurodegenerative metabolic disease. Nat. Med. 13, 439–447.

51. Jeyakumar, M., Norflus, F., Tifft, C.J., Cortina-Borja, M., Butters, T.D., Proia, R.L., Perry, V.H., Dwek, R.A., Platt, F.M., Tiff, C.J., et al. (2001). Enhanced survival in Sandhoff disease mice receiving a combination of substrate deprivation therapy and bone marrow transplantation. Blood 97, 327–329.

52. Ricca, A., Rufo, N., Ungari, S., Morena, F., Martino, S., Kulik, W., Alberizzi, V., Bolino, A., Bianchi, F., Del Carro, U., et al. (2015). Combined gene/cell therapies provide long-term and pervasive rescue of multiple pathological symptoms in a murine model of globoid cell leukodystrophy. Hum. Mol. Genet. 24, 3372–3389.

53. Visigalli, I., Moresco, R.M.R.M., Belloli, S., Politi, L.S.L.S., Gritti, A., Ungaro, D., Matarrese, M., Turolla, E., Falini, A., Scotti, G., et al. (2009). Monitoring disease evolution and treatment response in lysosomal disorders by the peripheral benzodiazepine receptor ligand PK11195. Neurobiol. Dis. 34, 51–62.

54. Capotondo, A., Milazzo, R., Salvatore, L., Quattrini, A., Palini, A., Plati, T., Politi, L.S., Quattrini, A., Palini, A., Plati, T., et al. (2012). Brain conditioning is instrumental for successful microglia reconstitution following hematopoietic stem cell transplantation. Proc. Natl. Acad. Sci. U S A 109, 15018–15023.

55. Ballabio, A., and Gieselmann, V. (2009). Lysosomal disorders: from storage to cellular damage. Biochim. Biophys. Acta 1793, 684–696.

56. Lecommandeur, E., Cachón-González, M.B., Boddie, S., McNally, B.D., Nicholls, A.W., Cox, T.M., and Griffin, J.L. (2021). Decrease in myelin-associated lipids precedes neuronal loss and glial activation in the CNS of the sandhoff mouse as determined by metabolomics. Metabolites 11, 1–16.

57. Jeyakumar, M., Thomas, R., Elliot-Smith, E., Smith, D.A., Van der Spoel, A.C., d'Azzo, A., Perry, V.H., Butters, T.D., Dwek, R.A., Platt, F.M., et al. (2003). Central nervous system inflammation is a hallmark of pathogenesis in mouse models of GM1 and GM2 gangliosidosis. Brain 126, 974–987.

58. Porter, B.F., Lewis, B.C., Edwards, J.F., Alroy, J., Zeng, B.J., Torres, P.A., Bretzlaff, K.N., and Kolodny, E.H. (2011). Pathology of GM2 gangliosidosis in Jacob sheep. Vet. Pathol. 48, 807–813.

59. Baek, R.C., Martin, D.R., Cox, N.R., and Seyfried, T.N. (2009). Comparative analysis of brain lipids in mice, cats, and humans with Sandhoff disease. Lipids 44, 197–205.

60. Cachón-González, M.B., Wang, S.Z., Ziegler, R., Cheng, S.H., and Cox, T.M. (2014). Reversibility of neuropathology in tay-sachs-related diseases. Hum. Mol. Genet.

61. Haberland, C., Brunngraber, E., Witting, L., and Brown, B. (1973). The white matter in G M2 gangliosidosis. A comparative histopathological and biochemical study. Acta Neuropathol. 24, 43–55.

62. McNally, M.A., Baek, R.C., Avila, R.L., Seyfried, T.N., Strichartz, G.R., and Kirschner, D.A. (2007). Peripheral nervous system manifestations in a Sandhoff disease mouse model: nerve conduction, myelin structure, lipid analysis. J. Negat. Results Biomed. 6, 8.

63. Sango, K., Yamanaka, S., Ajiki, K., Tokashiki, A., and Watabe, K. (2002). Lysosomal storage results in impaired survival but normal neurite outgrowth in dorsal root ganglion neurones from a mouse model of Sandhoff disease. Neuropathol. Appl. Neurobiol. 28, 23–34.

64. Cachon-Gonzalez, M.B., Wang, S.Z., Lynch, A., Ziegler, R., Cheng, S.H., Cox, T.M., Cachòn-Gonzàlez, Wang, S.Z., Lynch, A., Ziegler, R., et al. (2006). Effective gene therapy in an authentic model of Tay-Sachs-related diseases. Proc. Natl. Acad. Sci. U S A 103, 10373–10378.

65. Cachon-Gonzalez, M.B., Wang, S.Z., McNair, R., Bradley, J., Lunn, D., Ziegler, R., Cheng, S.H., and Cox, T.M. (2012). Gene transfer corrects acute GM2 gangliosidosis–potential therapeutic contribution of perivascular enzyme flow. Mol. Ther. 20, 1489–1500.

66. Woodley, E., Osmon, K.J.L.L., Thompson, P., Richmond, C., Chen, Z., Gray, S.J., and Walia, J.S. (2019). Efficacy of a bicistronic vector for correction of sandhoff disease in a mouse model. Mol. Ther. Methods Clin. Dev. 12, 47–57.

67. Lahey, H.G., Webber, C.J., Golebiowski, D., Izzo, C.M., Horn, E., Taghian, T., Rodriguez, P., Batista, A.R., Ellis, L.E., Hwang, M., et al. (2020). Pronounced therapeutic benefit of a single bidirectional AAV vector administered systemically in sandhoff mice. Mol. Ther. 28, 2150–2160.

68. Niemir, N., Rouvière, L., Besse, A., Vanier, M.T., Dmytrus, J., Marais, T., Astord, S., Puech, J.P., Panasyuk, G., Cooper, J.D., et al. (2018). Intravenous administration of scAAV9-Hexb normalizes lifespan and prevents pathology in sandhoff disease mice. Hum. Mol. Genet. 27, 954–968.

69. Osmon, K.J.L., Woodley, E., Thompson, P., Ong, K., Karumuthil-Melethil, S., Keimel, J.G., Mark, B.L., Mahuran, D., Gray, S.J., and Walia, J.S. (2016). Systemic gene transfer of a hexosaminidase variant using an scAAV9.47 vector corrects GM2 gangliosidosis in sandhoff mice. Hum. Gene Ther. 27, 497–508.

70. Mingozzi, F., and High, K.A. (2013). Immune responses to AAV vectors: overcoming barriers to successful gene therapy. Blood 122, 23–36.

71. Oya, Y., Proia, R.L., Norflus, F., Tifft, C.J., Langaman, C., and Suzuki, K. (2000). Distribution of enzyme-bearing cells in GM2 gangliosidosis mice: regionally specific pattern of cellular infiltration following bone marrow transplantation. Acta Neuropathol. 99, 161–168.

72. Boelens, J.J., Prasad, V.K., Tolar, J., Wynn, R.F., and Peters, C. (2010). Current international perspectives on hematopoietic stem cell transplantation for inherited metabolic disorders. Pediatr. Clin. North Am. 57, 123–145.

73. Ferrari, G., Thrasher, A.J., and Aiuti, A. (2021). Gene therapy using haematopoietic stem and progenitor cells. Nat. Rev. Genet. 22, 216–234.

74. Begoña Cachón-González, M., Wang, S.Z., McNair, R., Bradley, J., Lunn, D., Ziegler, R., Cheng, S.H., and Cox, T.M. (2012). Gene transfer corrects acute GM2 gangliosidosis—potential therapeutic contribution of perivascular enzyme flow. Mol. Ther. 20, 1489–1500.

75. Martino, S., Marconi, P., Tancini, B., Dolcetta, D., De Angelis, M.G., Montanucci, P., Bregola, G., Sandhoff, K., Bordignon, C., Emiliani, C., et al. (2005). A direct gene transfer strategy via brain internal capsule reverses the biochemical defect in Tay-Sachs disease. Hum. Mol. Genet. 14, 2113–2123.

76. Sevenich, L. (2018). Brain-resident microglia and blood-borne macrophages orchestrate central nervous system inflammation in neurodegenerative disorders and brain cancer. Front. Immunol. 9, 1–16.

77. Liddelow, S.A., and Barres, B.A. (2017). Reactive astrocytes: production, function, and therapeutic potential. Immunity 46, 957–967.

78. Tremblay, M., and Sierra, A. (2014). Microglia in Health and Disease (Springer), p. 486.

79. Cachon-Gonzalez, M.B., Zaccariotto, E., and Cox, T.M. (2018). Genetics and therapies for GM2 gangliosidosis. Curr. Gene Ther. 18, 68–89.

80. Huang, J.Q., Trasler, J.M., Igdoura, S., Michaud, J., Hanai, N., and Gravel, R.A. (1997). Apoptotic cell death in mouse models of G(M2) gangliosidosis and observations on human Tay-Sachs and Sandhoff diseases. Hum. Mol. Genet. 6, 1879–1885.

81. Alonso-Pérez, J., Casasús, A., Gimenez-Muñoz, Á., Duff, J., Rojas-Garcia, R., Illa, I., Straub, V., Töpf, A., and Díaz-Manera, J. (2021). Late onset Sandhoff disease presenting with lower motor neuron disease and stuttering. Neuromuscul. Disord. 31, 769–772.

82. Hölzer, H.T., Boschann, F., Hennermann, J.B., Hahn, G., Hermann, A., von der Hagen, M., and Tüngler, V. (2021). Cerebellar atrophy on top of motor neuron compromise as indicator of late-onset GM2 gangliosidosis. J. Neurol. 268, 2259–2262.

83. Rowe, O.E., Rangaprakash, D., Weerasekera, A., Godbole, N., Haxton, E., James, P.F., Stephen, C.D., Barry, R.L., Eichler, F.S., and Ratai, E.-M. (2021). Magnetic resonance imaging and spectroscopy in late-onset GM2-gangliosidosis. Mol. Genet. Metab. 133, 386–396.

84. Masingue, M., Dufour, L., Lenglet, T., Saleille, L., Goizet, C., Ayrignac, X., Ory-Magne, F., Barth, M., Lamari, F., Mandia, D., et al. (2020). Natural history of adult patients with GM2 gangliosidosis. Ann. Neurol. 87, 609–617.

85. Wessels, M.E., Holmes, J.P., Jeffrey, M., Jackson, M., Mackintosh, A., Kolodny, E.H., Zeng, B.J., Wang, C.B., and Scholes, S.F.E. (2014). GM2 gangliosidosis in British Jacob sheep. J. Comp. Pathol. 150, 253–257.

86. Liu, Y., Hoffmann, A., Grinberg, A., Westphal, H., McDonald, M.P., Miller, K.M., Crawley, J.N., Sandhoff, K., Suzuki, K., and Proia, R.L. (1997). Mouse model of GM2 activator deficiency manifests cerebellar pathology and motor impairment. Proc. Natl. Acad. Sci. U S A 94, 8138–8143.

87. Kroll, R.A., Pagel, M.A., Roman-Goldstein, S., Barkovich, A.J., D'Agostino, A.N., and Neuwelt, E.A. (1995). White matter changes associated with feline GM2 gangliosidosis (Sandhoff disease): correlation of MR findings with pathologic and ultrastructural abnormalities. AJNR Am. J. Neuroradiol. 16, 1219–1226.

88. Ito, D., Ishikawa, C., Jeffery, N.D., Ono, K., Tsuboi, M., Uchida, K., Yamato, O., and Kitagawa, M. (2018). Two-Year follow-up magnetic resonance imaging and spectroscopy findings and cerebrospinal fluid analysis of a dog with Sandhoff's disease. J. Vet. Intern. Med. 32, 797–804.

89. Fumagalli, F., Calbi, V., Sessa, M., Zambon, A., Baldoli, C., Rancoita, P.M.V., Acquati, S., de Mattia, F., Tucci, F., Gallo, V., et al. (2020). Lentiviral hematopoietic stem and progenitor cell gene therapy (HSPC-GT) for metachromatic leukodystrophy (MLD): clinical outcomes from 33 patients. Mol. Genet. Metab. 129, S59.

90. Sessa, M., Lorioli, L., Fumagalli, F., Acquati, S., Redaelli, D., Baldoli, C., Canale, S., Lopez, I.D., Morena, F., Calabria, A., et al. (2016). Lentiviral haemopoietic stem-cell gene therapy in early-onset metachromatic leukodystrophy: an ad-hoc analysis of a non-randomised, open-label, phase 1/2 trial. Lancet 388, 476–487.

91. Gentner, B., Tucci, F., Galimberti, S., Fumagalli, F., De Pellegrin, M., Silvani, P., Camesasca, C., Pontesilli, S., Darin, S., Ciotti, F., et al. (2021). Hematopoietic stem-and progenitor-cell gene therapy for Hurler syndrome. N. Engl. J. Med. 385, 1929–1940.

92. Capotondo, A., Milazzo, R., Garcia-Manteiga, J.M., Cavalca, E., Montepeloso, A., Garrison, B.S., Peviani, M., Rossi, D.J., and Biffi, A. (2017). Intracerebroventricular delivery of hematopoietic progenitors results in rapid and robust engraftment of microglia-like cells. Sci. Adv. 3, e1701211.

93. Martino, S., Di Girolamo, I., Cavazzin, C., Tiribuzi, R., Galli, R., Rivaroli, A., Valsecchi, M., Sandhoff, K., Sonnino, S., Vescovi, A., et al. (2009). Neural precursor cell cultures from GM2 gangliosidosis animal models recapitulate the biochemical and molecular hallmarks of the brain pathology. J. Neurochem. 109, 135–147.

94. Schindelin, J., Arganda-Carreras, I., Frise, E., Kaynig, V., Longair, M., Pietzsch, T., Preibisch, S., Rueden, C., Saalfeld, S., Schmid, B., et al. (2012). Fiji: an open-source platform for biological-image analysis. Nat. Methods 9, 676–682.

95. Wrabetz, L., Feltri, M.L., Quattrini, A., Imperiale, D., Previtali, S., D'Antonio, M., Martini, R., Yin, X., Trapp, B.D., Zhou, L., et al. (2000). P(0) glycoprotein overexpression causes congenital hypomyelination of peripheral nerves. J. Cell Biol. 148, 1021–1034.

96. Noseda, R., Guerrero-Valero, M., Alberizzi, V., Previtali, S.C., Sherman, D.L., Palmisano, M., Huganir, R.L., Nave, K.A., Cuenda, A., Feltri, M.L., et al. (2016). Kif13b regulates PNS and CNS myelination through the Dlg1 Scaffold. PLoS Biol. 14, 1–26.

97. Samarani, M., Loberto, N., Soldà, G., Straniero, L., Asselta, R., Duga, S., Lunghi, G., Zucca, F.A., Mauri, L., Ciampa, M.G., et al. (2018). A lysosome–plasma membrane–sphingolipid axis linking lysosomal storage to cell growth arrest. FASEB J. 32, 5685–5702.

98. Valsecchi, M., Aureli, M., Mauri, L., Illuzzi, G., Chigorno, V., Prinetti, A., and Sonnino, S. (2010). Sphingolipidomics of A2780 human ovarian carcinoma cells treated with synthetic retinoids. J. Lipid Res. 51, 1832–1840.